Ancient permafrost and past permafrost in the Northern Hemisphere

Thomas Opel, Pascal Bertran, Guido Grosse, Miriam Jones, Marc Luetscher, Lutz Schirrmeister, Kim Stadelmaier, Alexandra Veremeeva

01818. Ancient permafrost and past permafrost in the Northern Hemisphere

Thomas Opel
Alfred Wegener Institute Helmholtz Center for Polar and Marine Research, Polar Terrestrial Environmental Systems Section, 14473 Potsdam, Telegrafenberg A 45, Germany
thomas.opel@awi.de

Pascal Bertran
Institut National de Recherches Archéologiques Préventives, 33130 Bègles, France, and PACEA, Université de Bordeaux-CNRS, allée Geoffroy-Saint-Hilaire, 33605 Pessac, France
Pascal.bertran@inrap.fr

Guido Grosse
Alfred Wegener Institute Helmholtz Center for Polar and Marine Research, Permafrost Research Section, 14473 Potsdam, Telegrafenberg A 45, Germany
Guido.Grosse@awi.de

Miriam Jones
Florence Bascom Geoscience Center, U.S. Geological Survey, 12201 Sunrise Valley Dr. MS926A, Reston, VA 20192 USA
miriamjones@usgs.gov

Marc Luetscher
Swiss Institute for Speleology and Karst Studies, Serre 68, 2300 La Chaux-de-Fonds, Switzerland
marc.luetscher@isska.ch

Lutz Schirrmeister
Alfred Wegener Institute Helmholtz Center for Polar and Marine Research, Permafrost Research Section, 14473 Potsdam, Telegrafenberg A 45, Germany
Lutz.Schirrmeister@awi.de

Kim H. Stadelmaier
Karlsruhe Institute of Technology (KIT), Institute of Meteorology and Climate Research Troposphere Research (IMKTRO), 76131 Karlsruhe, Kaiserstraße 12, Germany
kim.stadelmaier@kit.edu

Alexandra Veremeeva
Alfred Wegener Institute Helmholtz Center for Polar and Marine Research, Permafrost Research Section, 14473 Potsdam, Telegrafenberg A 45, Germany
aleksandra.veremeeva@awi.de

01818. Ancient permafrost and past permafrost in the Northern Hemisphere
for The Encyclopedia of Quaternary Science, Third Edition (Elsevier)

Thomas Opel[1], Pascal Bertran[2], Guido Grosse[3], Miriam Jones[4], Marc Luetscher[5], Lutz Schirrmeister[3], Kim H. Stadelmaier[6], Alexandra Veremeeva[3]

[1]Polar Terrestrial Environmental Systems Section, Alfred Wegener Institute Helmholtz Centre for Polar and Marine Research, Potsdam, Germany

[2]Inrap / PACEA, Université de Bordeaux, Pessac, France

[3]Permafrost Research Section, Alfred Wegener Institute Helmholtz Centre for Polar and Marine Research, Potsdam, Germany

[4]Florence Bascom Geoscience Center, U.S. Geological Survey, Reston, VA, USA.

[5]Swiss Institute for Speleology and Karst Studies, La Chaux-de-Fonds, Switzerland

[6]Institute of Meteorology and Climate Research Troposphere Research, Karlsruhe Institute of Technology, Karlsruhe, Germany

Key points/objectives box

- Provide a definition of ancient and past permafrost
- Discuss the characteristics of ancient and past permafrost
- Provide an overview on modeling of past permafrost and methods for dating and classification of ancient and past permafrost
- Present a short temporal and spatial overview of ancient and past permafrost in the Middle and High Northern Latitudes

Glossary:

Ancient permafrost: Permafrost that has persisted at a locality since the Pleistocene or earlier and is still present.

Beringia: Vast continuous landmass between the Eurasian ice sheet in the west and the Laurentide and Cordilleran ice sheets to the east, that remained unglaciated during the last glacial period.

Epigenetic permafrost: Permafrost formed at some later time than sediment or substrate deposition.

Marine Isotope Stage (MIS): Alternating warm and cool periods in the Earth's paleoclimate, deduced from oxygen isotope values derived from deep sea sediment core samples

Past permafrost: Permafrost of Late Pleistocene or older origin that no longer exists at a particular locality

Relict permafrost: Permafrost which is out of equilibrium with modern climate and is a relict of past colder climate conditions during the Pleistocene or Holocene.

Syngenetic permafrost: Permafrost formed at the same time as sediment or substrate deposition.

Key words
Alaska, Beringia, biostratigraphy, Canada, chronology, dating, Europe, ice wedge, modeling, Pleistocene, Pliocene, permafrost, sand wedge, Siberia, stratigraphy

Abstract
The existence and dynamics of permafrost depend on the prevailing climate conditions. Therefore, the study of ancient permafrost (existing since the Pleistocene or earlier) and past permafrost (Late Pleistocene or older permafrost that no longer exists) and their dynamics may inform about climate and environmental changes in the past. In this chapter, we provide a brief overview of characteristics, detection and dating methods of ancient and past permafrost, before presenting a spatial and temporal history of permafrost in the middle and high northern latitudes. While the first permafrost may have formed about 3 million years ago, the late Pliocene and Early Pleistocene were characterized by frequent thawing and new formation of permafrost. It was not until the Middle and Late Pleistocene that permafrost became more persistent and widespread due to prolonged cooling. The most ancient dated permafrost formed between 800 and 600 ka in Yukon/Canada and East Siberia. Interglacial warming after the last ice age has led to massive thawing of permafrost and large areas in Europe, Asia and America are now characterized by traces of past permafrost.

1. Introduction

Permafrost is a thermal phenomenon and defined as all ground that remains continuously at or below 0°C for two consecutive years. In general, the occurrence of permafrost is an indicator of cold climate. When permafrost is in equilibrium with climate, mean annual air temperatures are below 0°C. In many places, however, particularly along the southern limit of the modern northern permafrost region, permafrost is out of equilibrium with modern climate and is a relict of past colder climate conditions during the Pleistocene or Holocene. The long-term dynamics of permafrost, i.e. its formation, stability, and degradation, are strongly linked to climate variations. Cold climates may lead to the formation of permafrost and may increase its extent and thickness. Stable permafrost conditions can be related to cold climates or even climate transitions if the dominating ecosystem protects the permafrost. Warmer climates lead to instability and degradation of permafrost.
While broad-scale permafrost formation typically is associated with glacial cold periods and widespread permafrost degradation is typically linked with interglacials, these general patterns can fall apart on local to regional levels. Recent studies highlight the intricate response of permafrost to climate variability and change, with some permafrost formation even occurring under favorable conditions of interglacials (Wetterich et al., 2016; Treat and Jones, 2018), and, conversely, some degradation also occurring during warmer phases (interstadials) of glacial periods (Vaks et al., 2020). This suggests that the response of permafrost to climate variability is more complex than a direct response to mean air temperature changes and may be mediated by changes to orbital insolation and seasonality, ecosystem characteristics such as insulative peat layers or vegetation cover, precipitation timing and seasonal distribution, hydrology, or local disturbances such as fires, erosion, or thermokarst (Jones et al., 2023). Permafrost dynamics strongly depend on seasonal climate

characteristics, such as the timing and length of the frost period, timing and depth of snow, the timing and length of the thaw season, and summer rainfall and temperature. Seasonality (climatic difference between warm and cold seasons) is further enhanced by the degree of continentality (distance to oceanic moisture and thermal contrast between oceans and continent modulated by the presence or absence of vast ice sheets and sea-level variations), which can produce a more extreme permafrost response in interior continental regions. The interplay between climate and permafrost dynamics over time has led to complex temporal and spatial patterns of permafrost formation, stability and degradation.

Understanding the age of permafrost and its past distribution is important for paleoenvironmental reconstructions and for characterizing permafrost-ecosystem-climate interactions over long glacial-interglacial timescales as well as during times of rapid change. We distinguish between *ancient* permafrost and *past* permafrost. In accordance with Murton (2021), we define ancient permafrost as permafrost that has persisted at a locality since the Pleistocene or earlier and is still present. Past permafrost refers to permafrost of late Pleistocene (i.e. > Marine Isotope Stage (MIS) 2) or older origin that no longer exists at a particular locality (Murton, 2021).

Ancient permafrost is considered a major organic carbon pool (Jones et al., 2023; Strauss et al., this volume), a source of well preserved ancient biota ranging from sedimentary DNA to viable viruses, bacteria and protists to mammal macrofossils (e.g., Willerslev et al., 2014; Germonpré et al., 2017; Abramov et al., 2021; Cherbunina et al., 2021; van der Valk et al., 2021; Courtin et al., 2022; Alempic et al., 2023, Shatilovich et al., 2023). A quantitative assessment of its past distribution, persistence, and loss allows better assessing biogeochemical and biological risks for the currently rapidly warming permafrost regions (Miner et al., 2021). Furthermore, ancient permafrost and associated microbial ecosystems can be considered as a model of extraterrestrial habitats (Gilichinsky et al., 2002) and analogue of Martian permafrost (Miner et al., 2023).

Permafrost formation processes can have important implications when studying past and future permafrost. Syngenetic and epigenetic permafrost are differentiated based on the temporal relationship between deposition and freezing, which is important for some research questions, in particular for microbiological studies (Abramov et al., 2021), fate of permafrost carbon following thaw (Jones et al., 2023), and for paleoenvironmental investigations. Epigenetic permafrost forms after the host sediment or rock deposition occurs and the age of the permafrost therefore differs from the age of the sediments. There may be a time lag of thousands or even million of years between accumulation and perennially freezing of the deposits (French and Shur, 2010). Syngenetic permafrost forms simultaneously with sedimentation as the lowest part of the active layer freezes and permafrost aggrades upwards. Therefore, the age of the permafrost is equal to the age of the host deposits (French and Shur, 2010). However, many thick permafrost sequences can be viewed as polygenetic, partly consisting of both epigenetic and syngenetic permafrost.

In this chapter, we summarize the state of knowledge on permafrost dynamics in the Middle and High Northern Latitudes, i.e. north of ~35°N, since the late Pliocene, i.e., the last about 3.5 million years (Ma). We briefly (1) discuss characteristics and detection of ancient and past permafrost, as well as approaches to date ancient and past permafrost and (2) present a temporal and spatial overview of past and ancient permafrost dynamics.

2. Characteristics and detection of ancient and past permafrost

2.1. Ancient permafrost: Ice and sediment structures

Ancient permafrost has been studied for more than a hundred years in various areas of the Arctic and sub-Arctic in Siberia, the Russian Far East, in Alaska, in the Canadian Yukon

Territory, on Greenland, and Spitsbergen. Often, ancient permafrost is buried deep in the ground up to tens or hundreds of meters below the surface. The older and deeper these deposits are, the less accessible they are. Hence, ancient permafrost has been mostly studied using outcrop profiles at sea coasts or river and lake shores. Additionally, boreholes and permafrost cores, tunnels and open-cast mines have been investigated. In some cases, research tunnels have been excavated. Permafrost profiles are examined for diagnostic sediment and ice structures and sampled for further sedimentological, mineralogical, hydrochemical and paleoenvironmental analyses.

A diagnostic feature of continuously frozen permafrost deposits is the presence of ice wedges (Fig. 1 A, D). Polygonal thermal contraction cracking of the frozen ground in winter and subsequent freezing of snowmelt, snow and hoarfrost in frost cracks in spring leads to the formation of an ice vein and multiple repetitions of cracking, infilling and refreezing over many years to the formation of v-shaped ice wedges. Mostly, ice wedges contain additional sediment and organic components flushed in the frost crack with snowmelt. Depending on the availability of snowmelt and the rate of sediment accumulation, frost cracks may be filled completely with sediments. Wedges comprising alternating sediment and ice veins are called composite wedges (Fig. 1 A, C).

<Figure 1 near here>

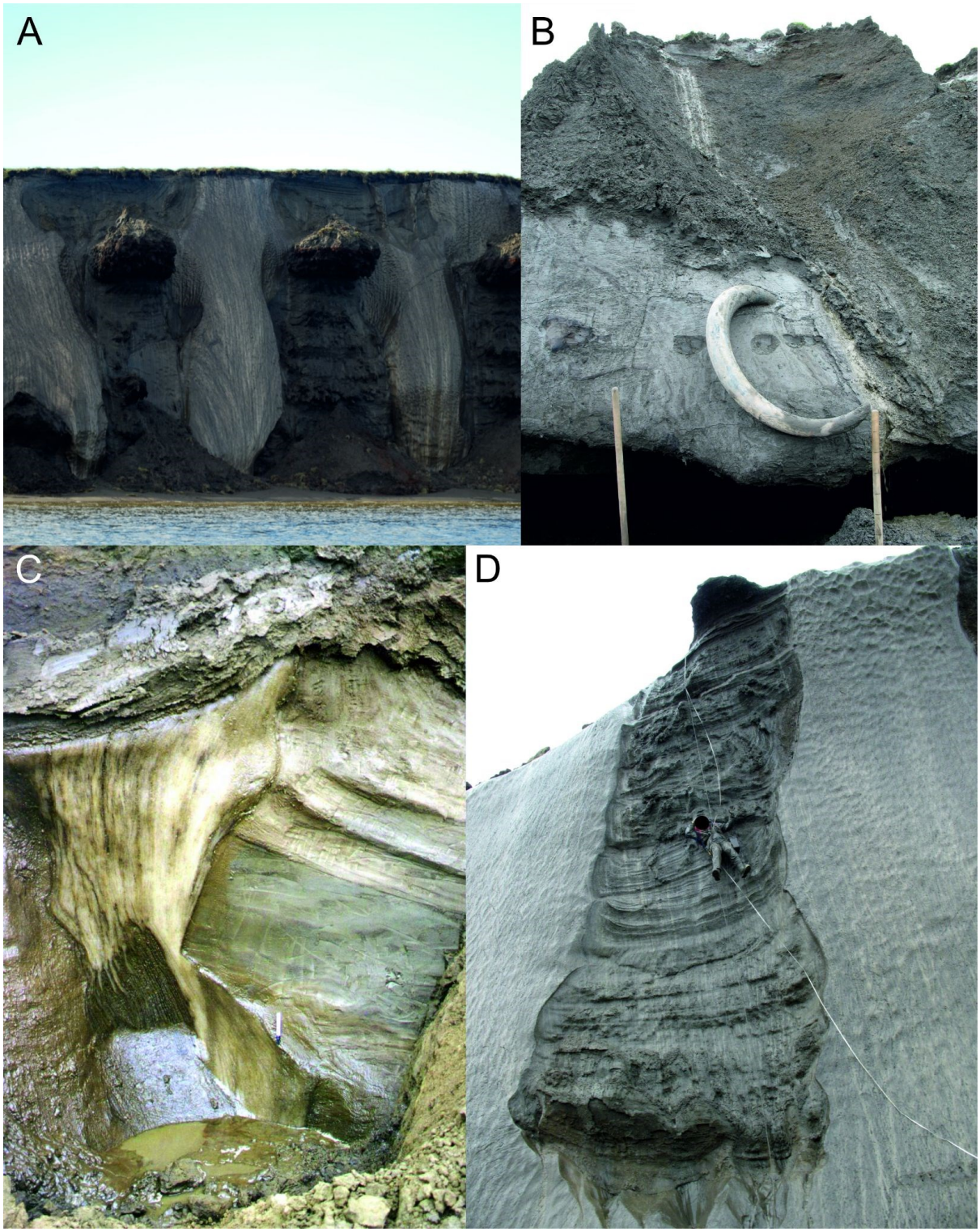

Fig. 1: View of permafrost exposure showing characteristic features of ancient permafrost. A: Syngenetic Late Pleistocene ice wedges at Sobo-Sise Island, Lena River delta, East Siberia with organic-rich sedimentary polygon fillings (cliff height 25 m). B: In-situ mammoth tusk (spade handle for scale; Oyogos Yar, East Siberia). C: Composite wedge with alternating ice and sediment veins transitioning upwards into an ice wedge (pen for scale) and thick ice belts (Bol'shoy Lyakhovsky Island, East Siberia). D: Sedimentary polygon filling with organic-rich layers and thick quasi-horizontal ice belts formed from moisture segregation (see person for scale, Bol'shoy Lyakhovsky Island, East Siberia). Photographs A and B: Thomas Opel, C and D: Lutz Schirrmeister

Ice wedges can grow synchronously with sediment accumulation (syngenetic ice wedges) or after sediment accumulation (epigenetic ice wedges). Ice wedges grow in polygonal patterns and may reach sizes of more than 20 m high and more than 5 m wide (Fig. 1 A, D). Epigenetic ice wedges are smaller and reach sizes of 1 to 4 m depth and 0.5 to 3 m width. Generally, wedge sizes vary according to thermal conditions, ground properties and the duration of growth.
Typically, syngenetically formed and continuously frozen deposits of the Pleistocene are silty fine sand to gravelly sand, sometimes with pebbles and often poorly sorted. Frozen peat inclusions or peat layers may be contained and also randomly distributed plant detritus. Epigenetic frozen sediments can also include layered silt and sand, depending on the specific depositional conditions, such as river or lake deposits.
Intra-sedimental ice structures diagnostic for continuously frozen conditions are massive (structureless), lenticular (horizontal or diagonal), layered, netlike reticulated ice structures, ice bands or belts up to several cm thickness (Fig. 1 D). The ice structures in frozen deposits depend, for example, on the rate of freezing, repeated freezing and thawing in the active layer and also on later transformational processes.
Besides describing sediment and ice structures, fossil bioindicators (e.g. pollen, plant macrofossils, ostracods, insects, and mammal bones) can be used to infer paleoenvironments and possibly the age of ancient permafrost using biostratigraphy (Fig. 1 B). Stratigraphically differentiating between warm interglacial and cold glacial periods and, within the cold periods, between stadial and interstadial intervals, can be performed by examining vegetation communities inferred from e.g. pollen. For example, a sparse grassy tundra was typical of stadial glacial periods in the Arctic lowlands of north-eastern Siberia. Interstadial periods were characterized by a steppe-like tundra with large herds of Pleistocene megafauna. Interglacial warm periods were characterized by shrub and forest tundra and even treed landscapes with evidence for numerous thermokarst lakes.

2.2. Past permafrost

2.2.1. Sediment structures and geomorphology

Various landforms and sedimentary features created by the growth and subsequent melting of perennial ground ice bodies are used to reconstruct the past permafrost extent. The most commonly used structures are ice wedge pseudomorphs (Fig. 2). The depression left by the melting ice wedges during permafrost thaw is filled by the subsidence of host or overlying sediments through colluviation, creep or rotational sliding (secondary fill). In present North America, ice wedges are mainly active in the tundra zone, in a context of continuous permafrost (e.g., Kokelj et al., 2014). In more southerly taiga regions with discontinuous to continuous permafrost, ground thermal contraction cracking rarely occurs because the thicker snow cover insulates the ground (Kokelj et al., 2007). For this reason, ice wedges are generally considered an indicator of continuous permafrost areas with a mean annual air temperature less than ca. -6°C, ground surface temperature at the time of cracking of at least -15°C and a strong thermal gradient in the upper meter of ground (Matsuoka et al., 2018) . Thermal contraction cracking can nevertheless occur in regions of deep seasonal frost when vegetation is reduced and snow cover is absent (e.g. Okkonen et al., 2020). Since the European Last Glacial Maximum (LGM) vegetation was largely dominated by steppe-tundra, the main factor limiting the formation of ice wedges was probably the ability of ice to subsist permanently in the ground for at least a few decades. Therefore, Pleistocene pseudomorphs are considered indicative of either continuous or discontinuous permafrost.

<Figure 2 near here>

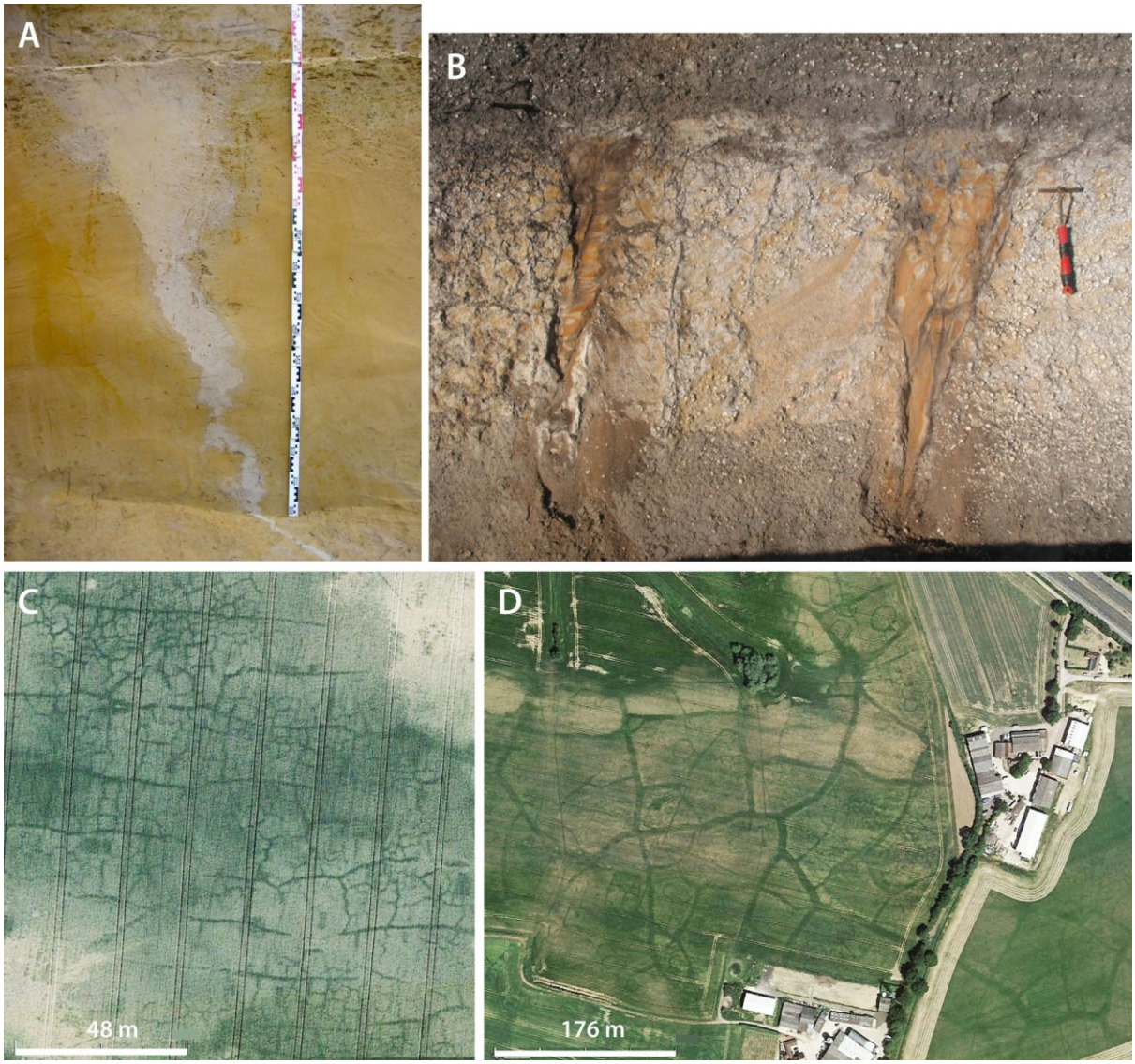

Fig. 2: View of sedimentary structures and landforms. A - ice wedge pseudomorph in Last Glacial loess, Curgies, France; the scale is 1.6 m (photo J.L. Locht); B - sand wedges in alluvial sand and gravel, Salaunes, France; the tool is 0.38 m long; C - subdivided orthogonal polygons, Dziewa, Poland (Google Earth); D - large mixed polygons, Great Milton, UK (Google Earth).

Wedges with primary fill (soil wedges, sand wedges) are not strictly diagnostic of permafrost, but more broadly of regions favorable to ground thermal contraction cracking. Soil wedges (usually called “frost cracks” in the geological record) result from the crumbling of crack edges or the infiltration of colluvial sediments into the cracks, and are characterized by a reduced width at the opening (typically less than 20 cm) and by the lack of evidence of collapse of host sediments. Sand wedges originate from the repeated accumulation of aeolian sand in cracks and develop in areas affected by deflation, particularly at the periphery of dune fields (Wolfe et al., 2018). Melting ice of composite wedges tends to erase the lamination and generate a massive fill. Other factors also contribute to this process, particularly subsequent bioturbation and freeze-thaw cycles, so the identification of composite wedge pseudomorphs remains highly uncertain.

At the ground surface, wedges are arranged in polygons 5 to 100 m in diameter (varying according to lithology, on average 15 m for Pleistocene Europe), which are easily visible from aerial and satellite photographs (e.g., Bertran, 2022) (Fig. 2). The morphology of polygons varies according to the dominant type of junction between the thermal contraction

cracks (T, X or Y-shaped), their degree of subdivision and the regularity of cracks. Regular orthogonal polygons result from the rectilinear propagation of cracks when the stress generated by thermal contraction is much higher than the frozen ground strength, usually in very cold regions with continuous permafrost. Pleistocene examples documented in Europe suggest that polygon development was rapid. The networks are clearly identifiable from aerial photographs in areas that were only subjected to thermal contraction cracking for two millennia. Mature polygons, i.e. polygons that no longer evolve significantly by subdivision, appear after about four millennia of cracking activity. Polygons associated with ice wedge pseudomorphs and relict sand wedges have similar characteristics in aerial view.
Scars of cryogenic mounds, lithalsas and pingos, are also good tracers of past permafrost. Their ramparts partially remain after the ice has melted. When the ramparts are severely degraded due to colluviation or deflation, only rounded depressions plugged by fine-grained lacustrine or peaty sediments remain.
Cryogenic calcite, formed by the precipitation of dissolved carbonates when water freezes, also provides a good indicator of the past existence of permafrost in specific environments (Žák et al., 2012). Precipitation can occur at the ground surface and in subsurface, generally as fine-grained crystals, in relation to icings and large ice lenses in a permafrost or deep seasonal frost context. In caves that are not subject to seasonal climate variations, coarse-grained cryogenic cave carbonate (i.e. calcite formed slowly in pools) is evidence of permafrost. The depth at which cryogenic calcite appears can be used to estimate permafrost thickness. Additionally, massive ice formations in caves provide evidence for permafrost.
Many other structures can give indications of past periglacial climates but are not necessarily proof of permafrost. These structures are related to the formation and melting of ice, generally as segregation lenses, and include frost-creep / gelifluction, cryoturbation and associated phenomena (patterned grounds). The thickness of the layer affected by cryoturbation and the size of patterned grounds are sometimes used to determine the presence of permafrost.
In addition to landforms and sedimentary structures, the concentration of dissolved noble gases in ancient groundwater can be used to determine the recharge temperature of aquifers (NGRT), as the solubility of noble gases is temperature-dependent and insensitive to biological and chemical processes (e.g., Seltzer et al., 2021). Coupled with ^{14}C dating of dissolved carbonates (after correction for dead carbon incorporation), it provides a paleothermometer and makes it possible to estimate fluctuations in near-surface ground temperature over the last 40 ka. In permafrost regions, infiltration occurs during thaw periods and the NGRTs measured in large aquifers range from 0°C to +1°C. In areas of continuous permafrost, infiltration decreases considerably due to ground sealing by ice leading to a recharge gap, although areas of recharge may subsist, e.g. under rivers and thermokarst lakes.
Recharge gaps can also be documented in speleothems in caves (Vaks et al., 2013). Periods without speleothem growth can indicate continuous permafrost above the cave that prevents meteoric waters to seep through the vadose zone, although other factors may limit water circulation as well (e.g., dryness). As speleothems can be precisely dated over hundreds of thousands of years, speleothem chronologies provide a detailed history of permafrost thaw and formation within a certain region and help constraining the chronology of long-term permafrost dynamics. This approach has been successfully utilized for study regions in Siberia, West Canada, and Greenland.

2.2.2. Modeling of past permafrost

Besides geomorphological evidence, climate model data can be used to derive permafrost occurrence that is in equilibrium with simulated climate conditions. A climate model is a computational tool built on the fundamental laws of physics to represent the complex interactions of Earth's atmosphere, oceans, land surface, and ice. Input of climate models are boundary conditions such as orbital parameters and solar forcing, atmospheric greenhouse gas concentrations, topography and ice sheets. After a spin-up phase of the model, the simulated climate is in equilibrium with the given boundary conditions and model output can be analyzed. This output comprises gridded climate parameters, as for example temperature, precipitation, soil temperatures on different depth levels, oceanic heat content, among many others (e.g., Steffen et al., 2020).

Typical horizontal resolutions in the paleoclimate modeling realm are 100 km - 200 km grid sizes for global climate models. Regional climate models are used to downscale the global model simulations for smaller regions of interest. Hence, the resolution is much higher (typically 10 km - 50 km) with more processes being explicitly resolved and the topographic effect being better captured. These higher resolutions may bridge the gap for direct model-proxy data comparison (Ludwig et al., 2019).

The derivation of permafrost from climate model data is based on either direct or indirect methods. For the direct permafrost detection, annual mean soil temperature of a certain depth is considered. Permafrost is assumed in locations where this temperature is below 0°C. Usually, the deepest available soil data (3 m - 40 m in recent paleoclimate models) is used (e.g., Slater and Lawrence, 2013). With this approach, it is not possible to distinguish between different types of permafrost (continuous, discontinuous, sporadic) and when the first climate models were developed, soil temperatures were not accurate enough to be used for permafrost derivation. Therefore, indirect methods were developed: The mean annual air temperature (MAAT) can be reconstructed from permafrost occurrence detected by geomorphological evidence. This fact can be used to infer permafrost occurrence from climate model data. Continuous permafrost is inferred where MAAT is below -8 ± 2°C and discontinuous permafrost is inferred where MAAT is between -8 ± 2°C and -4 ±2°C. Uncertainty ranges are introduced, because the values differ depending on the soil types and to account for effects of snow and vegetation cover (Vandenberghe et al., 2012). The most common indirect method to derive permafrost occurrence is the Surface Frost Index (SFI, Nelson and Outcalt, 1987). For this index, the cumulative days below 0°C (degree-days of freezing, DDF) and above 0°C (degree-days of thawing, DDT) are related as follows:

$$SFI = \sqrt{DDF} \;/\; (\sqrt{DDF} + \sqrt{DDT})$$

The SFI ranges between 0 and 1. An SFI above 0.67 indicates continuous permafrost, an SFI between 0.6 and 0.67 discontinuous permafrost and between 0.5 and 0.6 sporadic permafrost, below 0.5 no permafrost is indicated. Whereas the originating method was based on daily air temperatures above or below 0°C and several attempts were made to introduce snow cover effects, it became common to use soil temperatures instead where the effects of snow and vegetation are already taken into account by the climate models (Saito et al., 2013).

In addition to the permafrost detection, criteria for thermal contraction cracking can be applied on climate model data to test the potential growth of ice and sand wedges, enabling direct model-proxy data comparison. Derived from fieldwork in Svalbard, two criteria based on daily mean soil temperature data have to be fulfilled simultaneously in order to infer areas with thermal contraction cracking. For shallow cracking, potentially within the active layer or seasonally frozen ground, the daily mean soil temperature at a depth of 1 m (T_{100}) is required to be below -5°C when the temperature gradient in the upper meter of the ground (G_{AL}) is

below -7°C/m. For intensive deep thermal contraction cracking, the threshold values are T_{100} < -10°C and G_{AL} < -10°C/m.
Exact values of these criteria depend on e.g. the ice and organic carbon content and vary between different regions. Nevertheless, they allow estimates of areas with thermal contraction cracking (Stadelmaier et al., 2021).

2.3. Dating methods and stratigraphic classification for ancient and past permafrost

Once evidence of ancient or past permafrost has been discovered based on sedimentary and ice structures and geomorphology, it is crucial, but often difficult, to date using appropriate dating methods. In the following, we will briefly mention the most common dating methods for past and ancient permafrost deposits but refer for more details to the specific chapters on dating methods of this edition of the Encyclopedia of Quaternary Science (Elias, 2024). The age of past and ancient permafrost deposits of the MIS 3 or younger is usually determined by radiocarbon dating of included organic matter or optically stimulated luminescence (OSL) dating. Dating permafrost deposits devoid of organic matter and biogenic carbonates (e.g. gastropod shells) or beyond the range of radiocarbon, i.e. older than MIS 3, is more challenging. Methods successfully applied so far include OSL, infrared stimulated luminescence (IRSL) or thermoluminescence (TL) dating of quartz or feldspar grains (e.g., Murton et al., 2022), radioisotope disequilibria (^{230}Th/U) of peat (e.g., Schirrmeister et al., 2002; Wetterich et al., 2016), and ^{36}Cl/Cl ratios (Blinov et al., 2009) and ^{234}U/^{234}U activity ratios in ground ice (Ewing et al., 2015). Other methods applied to date or stratigraphically attribute middle Pleistocene and older permafrost deposits include paleomagnetics (e.g., Minyuk and Ivanov, 2011; Jensen et al., 2013) and biostratigraphy using distinct animal and plant fossils unique to specific time horizons. For example, based on evolutionary stages Sher (1974) used mammal remains while Repenning (1992) used rodent teeth for biostratigraphic classification in the Kolyma Lowland region permafrost and large-scale correlation. Preferentially, several dating methods should be applied, in particular for older deposits.
For permafrost deposits in western North America (Alaska, Yukon), tephrochronology plays an important role due to the proximity of major volcanic regions (e.g., Froese et al., 2009). Speleothems are usually dated using radiometric dating, i.e. U/Th and U/Pb (e.g., Vaks et al., 2013, 2020).

3. Temporal and spatial overview of past and ancient permafrost

3.1. Basic considerations

Over geological timescales, permafrost conditions on Earth have changed significantly in response to climate and environmental changes. Minimum or absent permafrost can be assumed for greenhouse states while icehouse states were characterized by larger permafrost extent. After tens of millions of years of global climate cooling during the Cenozoic (last ~66 million years (Ma), permafrost has redeveloped in the high latitudes of both hemispheres. The oldest reported age of permafrost formation relates to the middle Miocene (~15 Ma) for the Friis Hills inselberg in the McMurdo Dry Valleys of Antarctica (Verret et al., 2021), which arguably represents the most ancient permafrost on Earth. Permafrost formation in the high Northern Latitudes started substantially later (Fig. 3), presumably in the late Pliocene or Early Pleistocene as a response to further prolonged climate cooling (Jones et al., 2023). A late Pliocene onset of permafrost aggradation in Chukotka, northeastern Russia linked to the MIS M2 cooling event around 3.3 Ma has been inferred from pollen and element data of the Lake El'gygytgyn sediment core (Wennrich et

al., 2016) and is likely also for a few other Arctic regions. This is broadly in line with the modeling results of Guo et al. (2023) for the mid-Pliocene warm period (~3.264 to 3.025 Ma), which indicate that near-surface permafrost was spatially highly restricted and limited to the east Siberian uplands, the Canadian High Arctic Archipelago, and northernmost Greenland.

<Figure 3 near here>

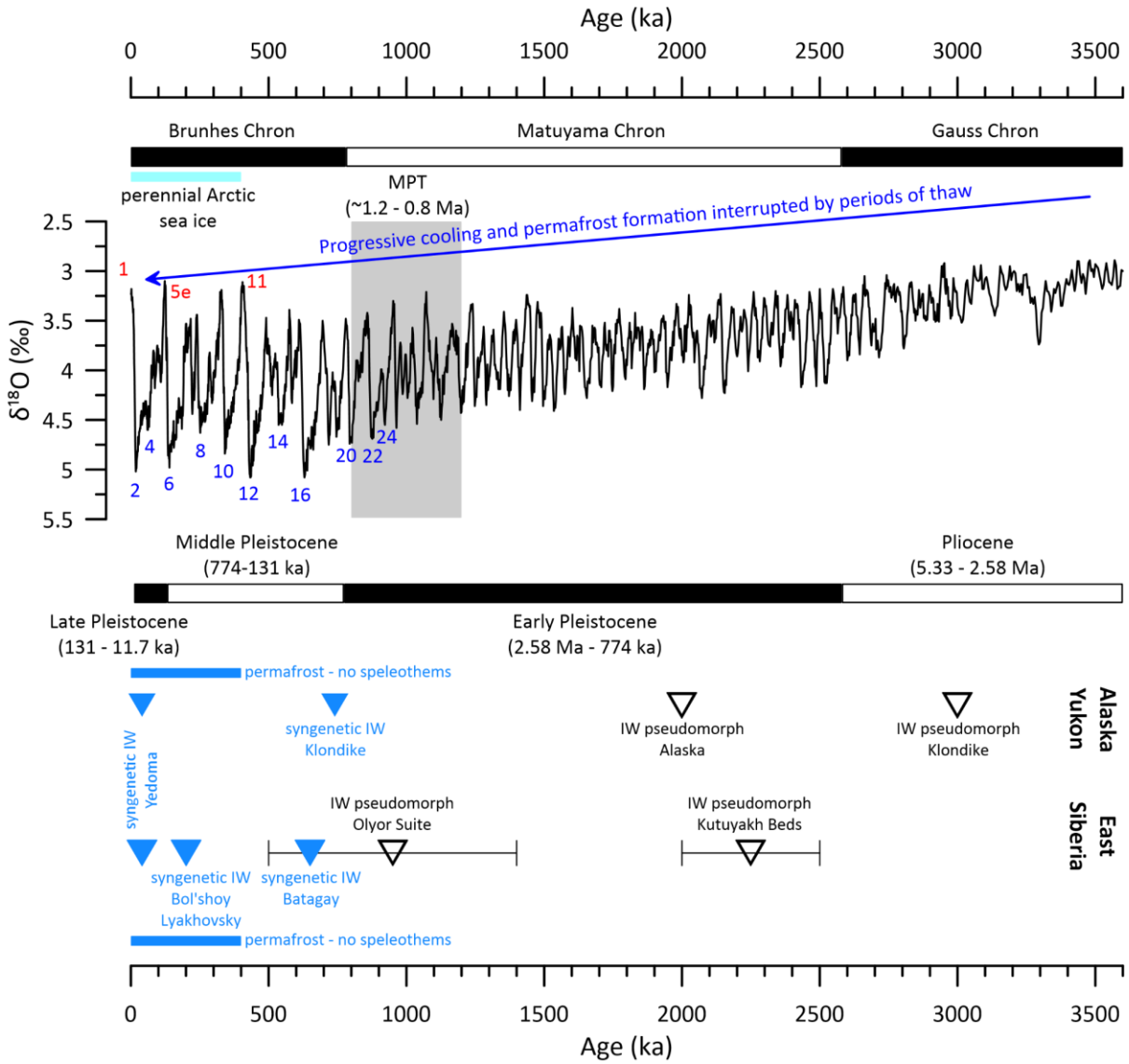

Fig. 3: Overview of major Northern High Latitude permafrost formation stages in response to long-term climate cooling. MPT: Mid-Pleistocene transition, IW: ice wedge, red numbers indicate major interglacials and blue number glacials of the last million years (modified after Murton, 2021).

The oldest dated evidence of past permafrost, i.e. ice wedge pseudomorphs in the Klondike (Yukon, Canada), yielded an age of ~3 Ma (Westgate & Froese, 2001), while the oldest ice wedge pseudomorphs in Alaska date to to the early Pleistocene ~2 Ma (Péwé et al., 2009) (Fig. 3). First ice wedge pseudomorphs in the Kolyma region in Northeast Siberia are attributed to the early Pleistocene period (2.4 to 1.9 Ma, Abramov et al., 2021). However, due to the lack of physical dating, the exact formation times remain vague.
It is likely that most of the early permafrost formations in the Northern Hemisphere have thawed and reformed at least one to multiple times during the late Pliocene and early Pleistocene. Only with prolonged climate cooling over the Pleistocene, vast permafrost

distribution could establish as evidenced by the most ancient physically dated syngenetic permafrost of the Northern Hemisphere that has persisted since at least the middle Pleistocene in the Klondike (Froese et al., 2008) and in the Yana Uplands (Batagay megaslump, Murton et al., 2022) (Fig. 3) even though ancient permafrost in the Kolyma region is assumed to be older (~1 Ma, Abramov et al., 2021) (Fig. 4). According to Chang et al. (2017), the first permafrost on the Qinghai–Tibet Plateau may have formed around 780-560 ka.

<Figure 4 near here>

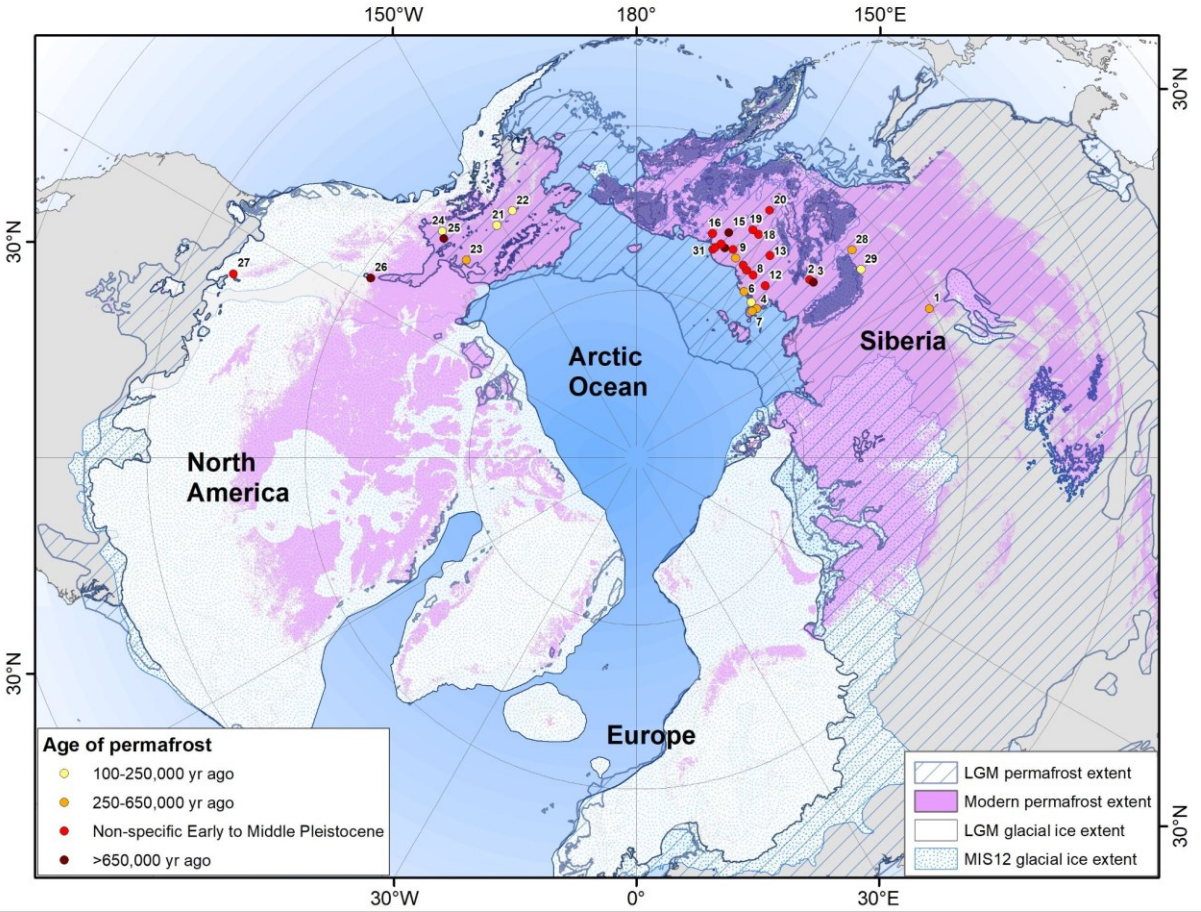

Fig. 4: Map of modern and last permafrost maximum permafrost region with sites of ancient permafrost older than 100 ka (modified after Jones et al., 2023): Modern permafrost (Obu et al., 2024), LGM permafrost (Vandenberge et al., 2014), glacial ice extent (Batchelor et al., 2019), sites of ancient permafrost (1 - Ledyanaya Lenskaya Cave, 2 - Adycha River, Ulakhan Sular section, 3 - Batagay Megaslump, 4 - Cape Svyatoy Nos, 5 - Oyogos Yar, 6 - Khaptashinskiy Yar, 7 - Bol'shoy Lyakhovsky Island, 8 - Achchagy-Allaikha site, 9 - Bolsh. Khomus-Yuryakh River, 10 - Keremesit River, 11 - Shandrin River, 12 - Khroma River, 13 - Badyarikha River, 14 - B. Chukochya River, 15 - Krestovka River, 16 - Cherskii site, 17 - Alazyea River, 18 - Sededema River, 19 - Slezovka River, 20 - Popovka River, 21 - Hess Creek, 22 - The Palisades Site, 23 - Northern Yukon Caves, 24 - Thistle Creek, 25 - Dominion Creek Site, 26 - Nahanni Plateau caves, 27 - Southern Canadian Rockies caves (Jones et al., 2023), 28 - Mamontova Gora (Cherbunina et al., 2021), 29 - Tumara River (Zech et al., 2013), 30 - Malaya Kon'kovaya River, 31 - Cape Maly Chukochy, 32 - Lake Yakutskoye (Shmelev et al., 2017).

The further we go back in time, the more fragmentary our knowledge of permafrost extent in the past becomes whereas we have a comparatively good understanding of the last widespread permafrost expansion during the late Pleistocene from MIS 4 to MIS 2, i.e. ca.

from 70 to 15 ka (Fig. 4). It can be assumed that massive permafrost degradation occurred mainly during the interglacials, i.e. the warmer than today Eemian (MIS 5e, 130-115 ka) and MIS 11 (424-374 ka), while new permafrost formed mainly during the cold glacials. Late glacial and Holocene warming caused massive warming of the permafrost, degradation and a significant reduction in permafrost thickness and extent, and transferred substantial parts of ancient permafrost into past permafrost, which is largely reflected in the distribution and characteristics of permafrost today (Jones et al., 2023) (Fig. 4). However, as ancient permafrost is often buried deep in the ground and therefore hard to study it is likely that there still exists older permafrost deeper in the ground of former Beringia. Beyond that it can be assumed that ancient permafrost still exists in some mountain regions under suitable conditions.
In the following we will discuss near-surface ancient and past permafrost deposits and characteristics. We focus mainly on (1) past permafrost in Europe, (2) ancient permafrost in East Siberia, and (3) ancient and past permafrost in North America, but also present information on ancient and past permafrost of the North-East of the European part of Russia and Western Siberia and the Qinghai-Tibet Plateau.

3.2. Europe

The distribution of past permafrost in Europe has been studied for more than a hundred years (Łozi´nski, 1912), and has been the subject of a number of studies in recent decades, giving rise to various reconstructions as field evidence accumulates, knowledge of present-day periglacial environments improves and paleoclimatic simulations are refined (Oliva et al., 2022). In general, the occurrence of past permafrost traces in West, Central, and East Europe is focused on the ice-free regions south of the Fennoscandian ice sheet and north of the Alps and the Carpathian mountain belt. In southern Europe, traces of past permafrost occur around and within the higher mountains (Oliva et al., 2022). The presence of ancient permafrost has only rarely been documented (Bartolomé et al., 2022).
The distribution map of ice wedge pseudomorphs (Fig. 5_A, from Andrieux et al., 2016, with additions) shows that all the ice-free regions of northern Europe were affected by permafrost during the Pleistocene glacials up to a latitude of ca. 48°N in France, and up to the Alpine Ice Sheet (ca. 47°N) in Germany. The southern limit of pseudomorphs is less well resolved in Central and Eastern Europe, due to fewer available data. The relict sand wedges, associated with composite wedge pseudomorphs (Buylaert et al., 2009), are clustered in the aeolian coversands that developed on the periphery of the Fennoscandian ice sheet (European Sand Belt). Relict sand wedges have also been documented in a latitudinal band to the south of the ice wedge pseudomorphs, between 43.5°N and 48°N in France and between 47°N and 48°N in Hungary (Farkas et al., 2023), in coversands and along rivers. These relict sand wedges are interpreted as features formed in a deep seasonal frost context unfavorable to the preservation of perennial ice bodies. Overall, the maximum size of the wedges decreases southwards (Fig. 6), in relation to temperature increase.

<Figure 5 near here>

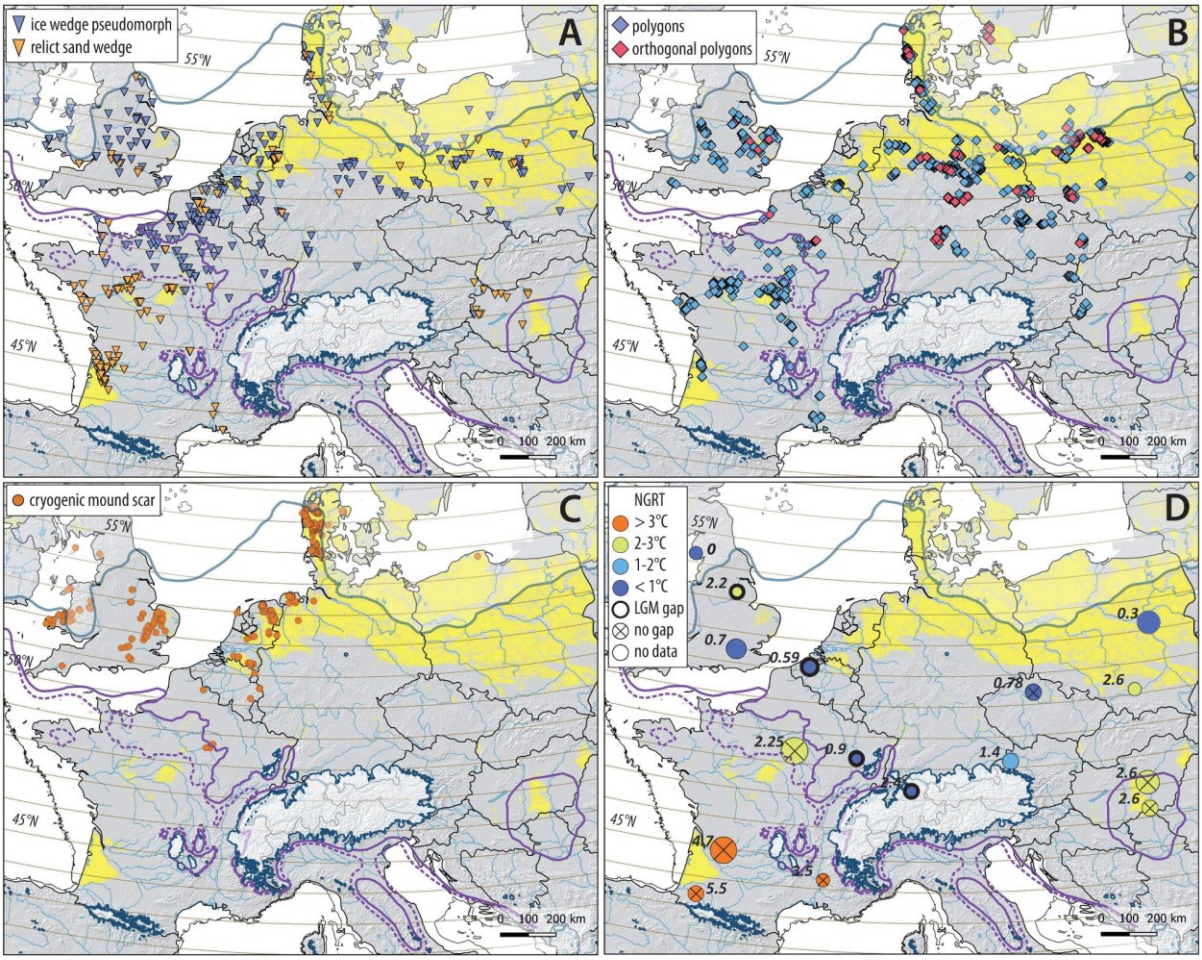

Fig. 5: Maps of past permafrost evidence in Europe. A – Distribution of ice wedge pseudomorphs and relict sand wedges (including composite wedges), from Andrieux et al. (2016) with additions; most (but not all) wedges are assumed to date from the Last Glacial Maximum (LGM); B – Distribution of polygonal cropmarks from satellite images (Bertran, 2022); C - Distribution of LGM to Lateglacial cryogenic mound scars from various authors; D – Lowest LGM Noble Gas Recharge Temperature of aquifers with indication of recharge gaps, from various authors. The solid purple line marks the extent of continuous permafrost and the dashed line the extent of discontinuous and sporadic permafrost from Bertran et al., (2022).

<Figure 6 near here>

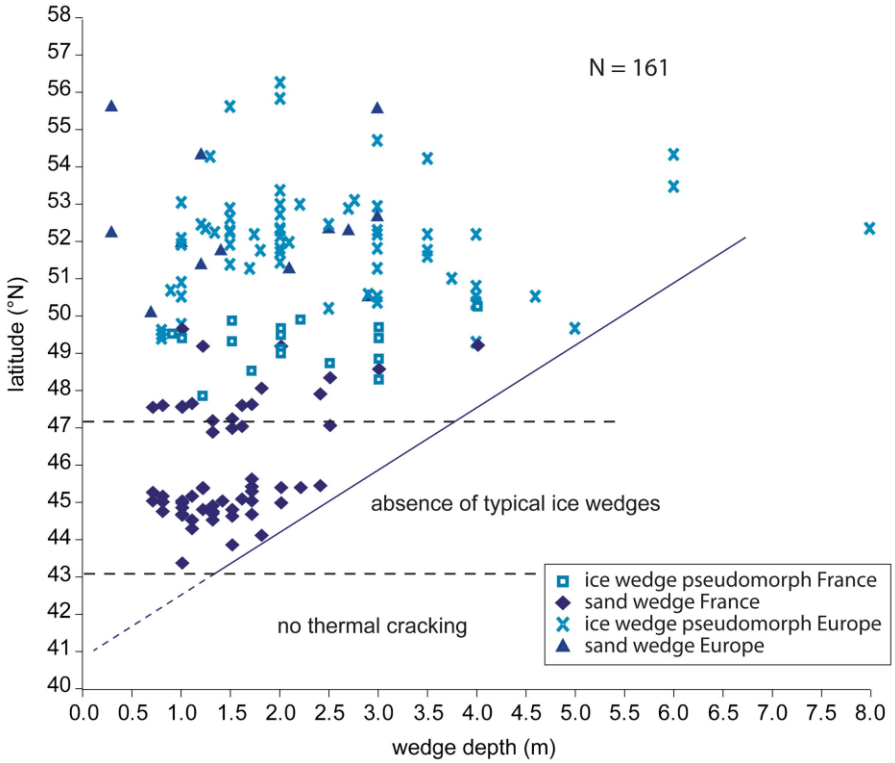

Fig. 6: Distribution of the depth of ice-wedge pseudomorphs and sand wedges in Europe as a function of latitude, from Andrieux et al. (2016). Pseudomorphs deeper than 6 m probably originate from syngenetic ice wedges.

<Figure 7 near here>

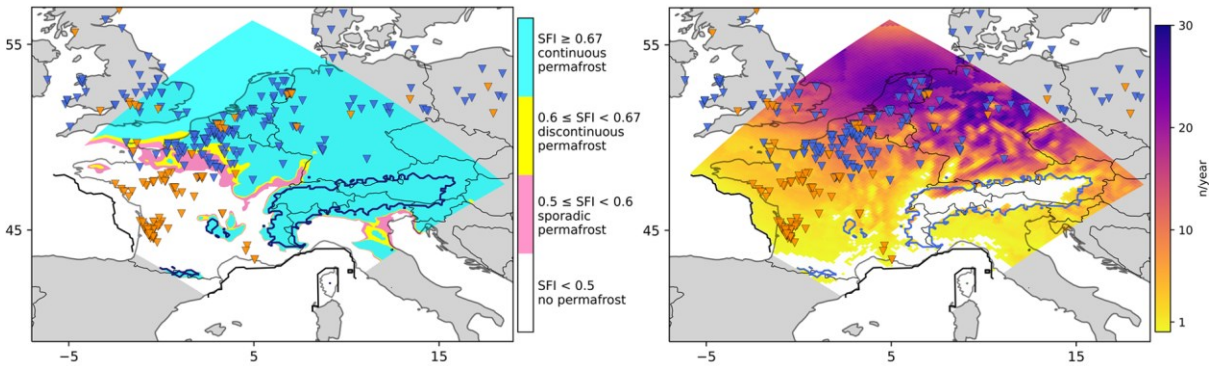

Fig. 7: Maps of simulated LGM permafrost (left) and heat maps with the mean number of days per year when the conditions for ground thermal contraction cracking are fulfilled (right). Thick black (blue) lines indicate the implemented coast line (ice sheet). The simulation was conducted with a 12.5 km grid spacing for the depicted area. Further modeling details are described in Stadelmaier et al., 2021. Blue and orange triangles indicate ice wedge pseudomorphs and relict sand wedges from Andrieux et al., 2016 and Isarin et al., 1998.

High-resolution regional climate model simulated for central Europe during the LGM shows the distribution of permafrost extent using the SFI (Fig. 7). Discontinuous and sporadic permafrost are rarely detected, possibly because the method is not well calibrated to LGM conditions (Vandenberghe et al., 2014), but the overall permafrost extent agrees well with the distribution of ice wedge pseudomorphs.
The mean number of days per year when conditions for ground thermal contraction cracking are fulfilled decrease to the south (Fig. 7_B); nevertheless, the criteria are fulfilled much

farther south than the detected permafrost extent, which again supports the view that relict sand wedges are an indicator for seasonally frozen ground.
The distribution map of polygons based on satellite photographs (Fig. 5_B) shows a pattern similar to that of ice wedge pseudomorphs and relict sand wedges, with distinct clusters mostly related to ground lithology. Polygons are virtually absent in the main loess areas because the pseudomorph networks are covered by loess layers deposited in a milder context at the end of the Last Glacial. The regular orthogonal polygons, which indicate very cold climates, are only found at latitudes of 50°N and above.
Few ice wedge pseudomorphs have been dated. Data available from loess-paleosol sequences indicate two main periods of ice wedge growth during the Last Glacial, corresponding to MIS 4, around 60 ka, the transition MIS3 - MIS2 and early MIS2, i.e. between 31 and 21 ka (e.g., Meijs, 2011). The oldest documented pseudomorphs come from the Leipzig region (Germany) and date from the early Pleistocene on the basis of stratigraphic evidence (Eissmann, 2002). In France, single grain OSL ages indicate that sand wedge growth occurred in discrete phases separated by long periods of inactivity throughout the Last Glacial, with a peak between 25 ka and 12 ka reflecting the main period of aeolian sand deposition (Andrieux et al., 2018). A few samples have also yielded ages dating back to the Penultimate Glacial (Saalian).
Many ramparted depressions in non-glaciated areas of Europe are interpreted as scars of Pleistocene cryogenic mounds (e.g., Ballantyne and Harris, 1994). When the rampart has been eroded, the distinction between depressions caused by the degradation of ice-rich permafrost (alases) and cryogenic mounds remains difficult. However, the hypothesis of permafrost-related landforms (thermokarst) remains widely accepted. The map (Fig. 5_C) illustrates the distribution of these landforms. The distribution shows a concentration north of latitude 51°N, mainly in northwestern Europe. Many of these structures still have a rampart and are, therefore, relatively recent (late Glacial). The structures located in the Paris basin, France, do not exceed latitude 48°N and lack ramparts because of subsequent erosion.
Data on noble gas recharge temperatures (NGRTs) of aquifers remain scarce in Europe. Fig. 5_D indicates the coldest NGRTs measured in some aquifers. The map shows that NGRTs below 1°C, likely associated with permafrost, are located in northern European countries. A recharge gap, linked to the virtual absence of infiltration during the LGM, has also been observed in some of these aquifers. In the Paris Basin (ca. 48°N) and the Pannonian Basin in Hungary (ca. 47°N), the recorded NGRTs range from 2 to 3°C with no identifiable recharge gap, which argues for the absence of continuous permafrost. Further south in France, the NGRTs are above 3°C and suggest the total lack of permafrost.

3.3. North-East of the European part of Russia and Western Siberia

Permafrost evolution of the NE European part of Russia and Western Siberia has similar geological and geomorphological conditions. The Pechora Lowland east and the West Siberian Plain west of the Ural Mountains have a plain low-elevated relief which predetermined climate conditions and formation of permafrost. The development of permafrost in this region differs from other Arctic regions due to transgressions and simultaneous maximum glaciations in the middle and late Pleistocene, caused by neotectonic movements (Gusev et al., 2012a). Specific to West Siberia is the vertical permafrost differentiation from north to south (Shpolyanskaya, 2015). In contrast to Yamal and Gydan peninsulas, between 60 and 64°N, Western Siberia and Pechora Lowland are characterized by a vertical double-layer structure with Holocene permafrost at the surface (up to 10-100 m) and below a thawed layer, relict permafrost from 100 up to 400 m. Southern regions of Western Siberia have only relict

permafrost existing at depths from about 100 to 300 m revealed by drilled boreholes (Zemtsov and Shamakhov, 1993).
Permafrost has formed since the Early Pleistocene in several stages related to transgressions and glaciations in this region (Svendsen et al., 2004; Nazarov et al., 2021). Recent OSL and paleofaunistic studies have significantly corrected the chronology of deposits since the Middle Pleistocene (Nazarov et al., 2021).
During the middle Pleistocene marine transgression, synchronous with the maximum glaciation, permafrost should have existed south of 60°N down to 54°N with a modeled thickness of 400-600 m (Shpolyanskaya, 2015). The origin of the oldest exposed deposits of the Sanchugovskaya Beds (Nikitinsky Yar near Ust-Port, Vorontsovo settlement, and outcrops on Severnaya Zemlya archipelago) is still debated: either marine or glacial-marine origin as suggested by findings of in-situ cold-water mollusks and syngenetic cryostructures (Gusev et al., 2012b; Shpolyanskaya, 2015) or a glacial origin correlated with related to the Samarovo glaciation till (MIS 8; Nazarov et al., 2021).
During MIS 5, continuous permafrost formed only north of the polar circle on islands in the today Kara Sea area with epigenetic freezing (Shpolyanskaya, 2015; Streletskaya et al., 2021). This led to complex cryostratigraphy, characterized by marine deposits with massive tabular ground ice (MTGI) overlain by coastal-marine deposits with polygonal ice wedges or epigenetic sediments with texture-forming ice. Deposits with MTGI overlain by sediments with reticular cryostructure are found at the Gydan Peninsula, in the Tadibeyakha River valley, and near Lake Ney-To on the Yamal Peninsula (Shpolyanskaya, 2015).
The cooling climate during Early Zyryan glacial time (MIS 4) led to permafrost formation in the northern part of Western Siberia with a thickness of up to 400-500 m. The glaciation partly formed permafrost deposits in its marginal parts. The Ledyanaya Gora site at the Yenisei River on the polar circle is likely buried ice of the Putorana Glaciation (Shpolyanskaya, 2015). During the MIS 3 interstadial permafrost formation continued. Sediments with MTGI were thought to be either buried glacial ice (e.g. Astakhov, 1996) or formed by non-glacial processes, such as initial subsea genesis and pure ice of coastal-marine genesis (Shpolyanskaya, 2015). Streletskaya et al. (2021) based on isotope and geochemical analyses concluded that the MTGI to be formed by epigenetic freezing of shallow marine sediments immediately after sea regression in the tidal zone .
During the Sartan glaciation (MIS 2) and significant sea level regression, the Kara Sea shelf was exposed to an isobath of 100-120 m (Pavlidis et al., 1997). Permafrost was widespread in vast areas with thickness up to 500 m (Shpolyanskaya, 2015). Terrestrial ice-rich polygenetic sediments with syngenetic and epigenetic ice wedges of MIS 3-2 age are present in the upper part of several outcrops of the Kara Sea coast (Streletskaya et al., 2021).

3.4. East Siberia

The oldest known permafrost deposits of entire Eurasia are located in the lower Kolyma region at the key site on the Krestovka River but also at other regional sites such as Alazyea River, and Bolshaya Chukochya River in their middle stream (Sher, 1997) (Fig. 4). The age attribution is based on biostratigraphy, i.e. evolution stages of microtine rodents (Repenning, 1992) and mammal fauna association (Sher, 1974) and mammoth DNA molecular clock dating (van der Valk et al., 2021), supported by paleomagnetic evidence (Minyuk and Ivanov, 2011). However, absolute dating results are not available. The first evidence of frost cracking could be identified in the sands and gravels of the Begunov Suite deposited between about 3.4 and 3 Ma in a forested environment (Giterman et al., 1982). However, they are not interpreted as permafrost but as a result of deep seasonal frost. The overlying

deposits of the Kutuyakh beds (about 2.5 to 2 Ma) (Fig. 3) show the oldest ice wedge pseudomorphs that are several meters deep. Progressive cooling has led to the development of a cold climate with actively aggrading and stable permafrost and the appearance of lowland tundra plant, insect, and mammal communities (Giterman et al., 1982; Sher, 1997). This permafrost thawed at least once as a result of regional warming before the overlying deposits of the Olyor Suite were deposited above an erosional unconformity (Giterman et al., 1982). The Olyor Suite (about 1.4 to 0.5 Ma) (Fig. 3) represents a major stage of Beringian mammal fauna (Olyorian Land Mammal Age) based on the evolutionary succession of collared lemming. Lower and upper boundaries show unconformities and have not yet been precisely defined (Sher, 1997) leading to different age attribution and interpretations for several sites with Olyor deposits (Repenning and Brouwers, 1992). It covers both the Matuyama-Brunhes reversal of polarity and Middle Pleistocene Transitions, i.e. the shift from ~41 kyr to ~100 kyr climate cycles. At the Kolyma River, the Olyor Suite accumulated under stable permafrost conditions (Sher et al, 1979) but ice wedge pseudomorphs with varying characteristics indicate a more complex sequence of permafrost aggradation and degradation (Giterman et al., 1982). The polarity shift from Matuyama to Brunhes allowed Minyuk and Ivanov (2011) to correlate deposits of the Olyor Suite over large parts of West Beringia, from Yakutia to Chukotka (Fig. 4).

Permafrost first appeared in the Ledyanya Lenskaya Cave in central eastern Siberia around 1.35 Ma (Vaks et al., 2020), at about the same time as the onset of permafrost aggradation of the Olyor Suite further north. The speleothem record for this cave shows intermittent speleothem growth and hiatuses without speleothem deposition, suggesting no permafrost and continuous permafrost above the cave, respectively, until about 400 ka. After the MIS 11 interglacial (429±23 ka), there was no speleothem growth at all, which indicates persisting continuous permafrost conditions, potentially related to the establishment of perennial sea ice in the Arctic Ocean (Fig. 3).

The most ancient physically dated permafrost with still existing syngenetic ice wedges was found in the Yana Highlands of East Siberia (Batagay Megaslump). The lowermost stratigraphic unit (Lower Ice Complex with huge ice wedges) exposed at the base of the about 55 m high headwall of this rapidly developing thaw slump could be dated to at least 650 ka (potentially MIS 17/16) (Fig. 3) using luminescence and ^{36}Cl/Cl dating (Murton et al., 2022) (Fig. 8). It has survived both the warm MIS 11 and 5e interglacials even though a thaw unconformity and erosional surface on the top indicate at least one permafrost degradation event sometime between MIS 16 and 7/6.

<Figure 8 near here>

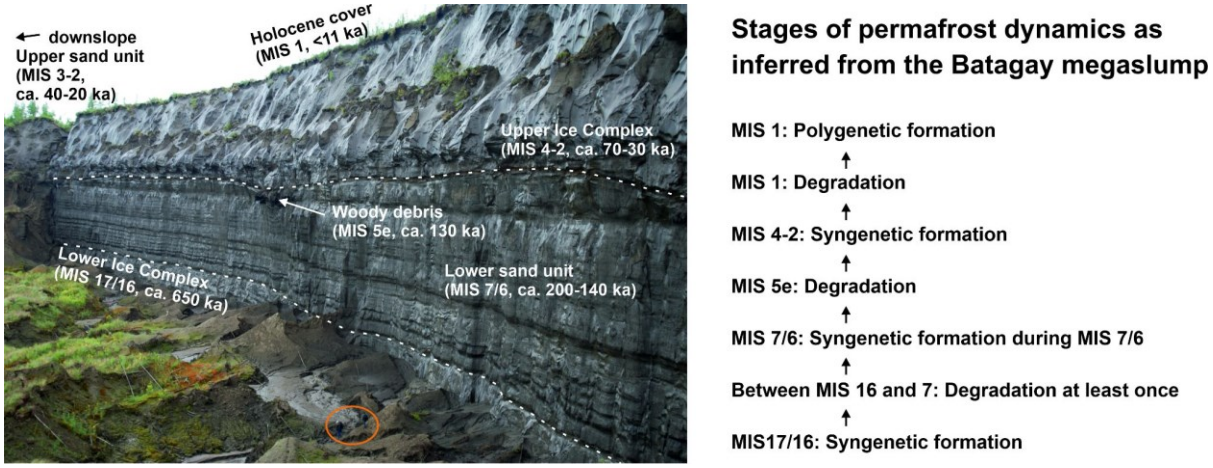

Fig. 8: Headwall of the Batagay Megaslump with cryostratigraphic units, obtained ages (Murton et al., 2022), and inferred stages of permafrost dynamics since the Middle Pleistocene. Orange circle: persons for scale. Photograph: Thomas Opel

Middle Pleistocene permafrost formation at some time after MIS 11 is known for several sites in interior Yakutia. At the Adycha River, permafrost is dated to 360±17 ka (Germonpré et al., 2017). At the Aldan River, sands of the Mamontova Gora exposure show evidence of syngenetic frost cracking and are attributed to the Middle Pleistocene based on mammal bone remains. Thermoluminescence ages of 300±5.7 ka and 176±2 ka confirm this (Cherbunina et al., 2021), while much older deposits of the Miocene-Pleistocene boundary below are frozen only epigenetically. Permafrost deposits of MIS 7-6 origin are reported for the Tumara loess-paleosol sequence west of the Verkhoyansk Mountain Range, too (Zech et al., 2013). Also, the syngenetic lower sand unit of the Batagay Megaslump is dated to MIS 7-6.

In Northern Yakutia, the syngenetic ice-rich Yukagir Ice Complex of Bol'shoy Lyakhovsky Island has been dated to the MIS 7 using ^{230}Th/U dating of peat and paleomagnetics (Schirrmeister et al., 2002; Wetterich et al., 2019). Middle Pleistocene syngenetic and epigenetic permafrost formation has been inferred for several North Yakutian sites (i.e., Cape Svyatoi Nos, Bol'shoy Khomus Yuryakh River, Khaptashinsky Yar, Achchagyi-Allaikha), based on ^{36}Cl/Cl ratios of wedge or segregation ice (Blinov et al., 2009) but large dating uncertainties and stratigraphic irregularities ask for independent age control. At the Dmitry Laptev Strait (Bol'shoy Lyakhovsky Island and Oyogos Yar), a complex pattern of formation (Buchchagy Ice Complex, Kuchchugui unit) and degradation (Krest Yuryakh unit) of ice-rich permafrost during MIS 5 *sensu lato* has been found. Dating results partly contrast stratigraphic interpretation (Wetterich et al., 2016; Opel et al., 2017) and ask for more physical dating.

The pronounced warming attributed to the Last Interglacial (MIS 5e) led to large-scale permafrost degradation throughout eastern Siberia manifested in erosive unconformities and widespread thermokarst lake deposits and ice wedge pseudomorphs, although older permafrost deposits buried deep underground were preserved. However, physical dating of respective deposits is missing and age attribution is based on stratigraphic interpretation and paleoecological reconstructions (Ashastina et al., 2018; Kienast et al., 2011) yet.

The significant cooling of the climate in the Late Pleistocene has led to a new phase of large-scale permafrost formation. In large parts of eastern Siberia, the ice-rich syngenetic deposits of the Yedoma Ice Complex have formed between MIS 4 and MIS 2 and large parts degraded during the Late Glacial and Holocene warming. Details are given in Schirrmeister et al. (this volume).

3.5. North America and Greenland

Some of the oldest permafrost in North America has been preserved outside of or within the corridor between the Laurentide and Cordilleran ice sheet margins of the LGM. Relict ice wedges in the discontinuous permafrost zone at Dominion Creek in the Klondike (Yukon Territory, Canada) (Fig. 4) just a few meters below the surface suggests permafrost has survived for at least 740 ka, including through two exceptionally warm interglacials (MIS 11 and 5e) (Froese et al., 2008) (Fig. 3). Persistence of relict ice wedges through the last interglacial at Thistle Creek a in the Yukon, Canada and the Palisades on the central Yukon River, Alaska within the discontinuous permafrost zone suggests they have remained protected because of their depth and overburden that protects permafrost from surface temperature fluctuations (Reyes et al., 2010).

Speleothem (cave drip) deposits from the northern Yukon to the southern Canadian Rockies suggest a stabilization of permafrost over the last 400,000 years (Fig. 3) consistent with a Pleistocene climatic cooling trend, development of perennial Arctic sea ice, and a change in the orbital pacing of glacial-interglacial cycles to 100,000-year cycles, but permafrost presence inferred from speleothems indicates it existed in the high Arctic from at least 1.5 to 0.5 Ma ago (Biller-Celander et al., 2021).

Studying a cave in the ice-free Northeast of Greenland, a region today characterized by extensive deep permafrost, Moseley et al. (2021) reconstructed speleothem growth related to permafrost-free conditions above the cave between ca. 588 and ca. 549 ka during MIS 15a (suggesting a warmer and wetter Arctic climate than today) and MIS 14. Absence of permafrost during this period is in line with speleothem chronologies in East Siberia at 60°N (Vaks et al., 2020).

Even though much of the thick permafrost on the Arctic Coastal Plain of Alaska has not been dated, much older evidence for permafrost can be found in features from Alaska (Fig. 4), which has remained largely unglaciated through the late Cenozoic (Péwé et al., 2009). These older deposits, which all have evidence of having thawed at some point since initial formation but have subsequently refrozen (epigenetic permafrost), are either visible at the surface because of river-cut bluffs, mining operations, or by engineered tunneling into permafrost. The Palisades bluff on the Yukon River in central Alaska exposes over 2 million year old history of permafrost, as determined by tephrochronology, preserving the most continuous record of Plio-Pleistocene terrestrial stratigraphy for the region (Matheus et al., 2003). Ice wedge pseudomorphs found beneath a tephra dated to 2 Ma ago indicate the presence of permafrost just prior to that time (Fig. 3). The nearly 3 million year old Gold Hill cut near Fairbanks, Alaska was exposed due to mining efforts in the 1950s and is characterized by thick loess deposits, divided into three units based on unconformities attributed to warming, including the Dawson Cut Forest Bed Unconformity (>2 Ma) between the lower and middle unit and the Ester Interval Unconformity (<0.78 to >0.61 Ma) between the middle and upper unit (Péwé et al., 2009). The lower unit is ice poor and ice wedge pseudomorphs are not visible until the middle unit (>1 Ma). The unconformity between the massive Gold Hill loess and Goldstream Formation represents a major period of loess erosion when the climate was at least as warm as modern climate, if not warmer, with most, if not all permafrost thawing at that time. Most of the Gold Hill loess in the region eroded with the reformation of stream flow from glacial meltwater from the Alaska Range, and the only known preservation of it remains at Gold Hill (Péwé et al., 2009). The age of the unconformity is bracketed by the Eva Forest Bed (125 ka) and underlying Old Crow tephra (130 ka), and most, if not all, of the Gold Hill loess has refrozen in the last 100,000 years (Péwé et al., 2009). Loess from the Hess Creek site in Interior Alaska was dated using

$^{234}U/^{238}U$ to ~200 ka with an estimated uncertainty of an order of magnitude, and ice bodies preserved in the ice-rich loess likely date from the last glacial period (Ewing et al., 2015). Most of the ice-rich permafrost in the Hess Creek location is syngenetic with regions of epigenetic silt (Ewing et al., 2015). The permafrost from the Vault Creek site from the Chatanika River valley near Fairbanks (Fig. 9 A) reveals more than 90 ka of periglacial landscape dynamics, ranging from fluvial to eolian deposition (Schirrmeister et al., 2016). Its valley bottom position dominated by fluvial processes complicates the chronology, and complementary geochronological, cryolithostratigraphical, and paleoecological data suggests the Vault Creek tunnel deposits are younger than the Illinoian (300-130 ka ago).

<Figure 9 near here>

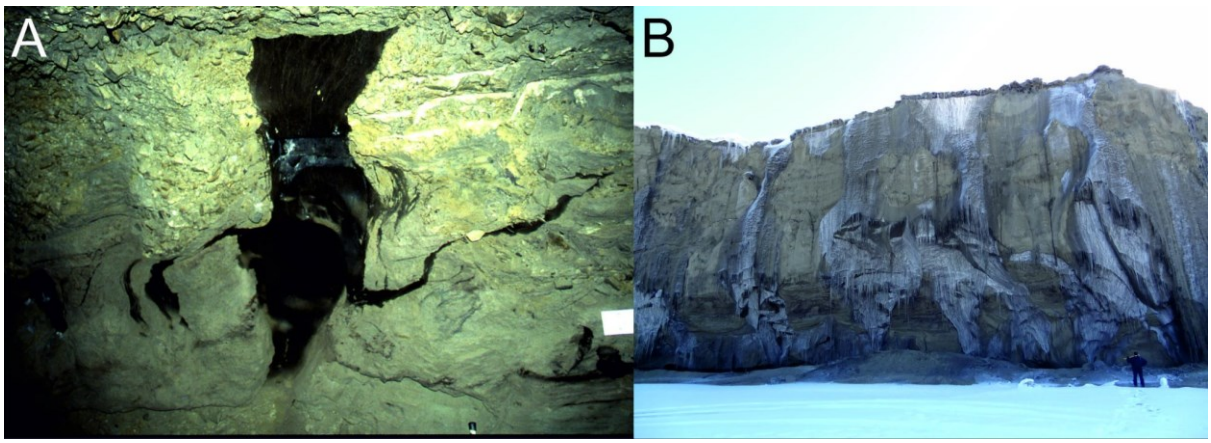

Fig. 9: A - Vault Creek (Alaska) tunnel with ice wedge (0.6 m wide) in gravel (OSL dated to 93.1±10.0 to 59.4±7.6 ka (Photograph Lutz Schirrmeister), B - Late Pleistocene Yedoma Ice Complex at the about 30 m high Itkillik exposure (Alaska North slope, see person for scale, Photograph Jens Strauss)

Generally, the Yedoma exposures in Alaska are much younger but some exceed the limits of radiocarbon dating. The Itkillik exposure on the North Slope of Alaska reveals continuous deposition of Yedoma for >48 ka (Fig. 9 B) with syngenetic ice wedges found throughout the stratigraphy, though micro-cryostructures dominate the exposure (Kanevskiy et al., 2011). The high ice volume is consistent with many Yedoma sites in East Siberia and can explain large depths of thaw-lake basins that formed in the region (Kanevskiy et al., 2011). The recently excavated new CRREL Permafrost Tunnel (Fox Tunnel) north of Fairbanks, Alaska expands on the old tunnel that was dug in the 1960s, exposing sediments nearly 43 ka old (Kanevskiy et al., 2022).

Past permafrost that extends beyond the limits of modern permafrost is determined by permafrost or periglacial features that remain on the landscape. While many of these features are not definitively indicative of past permafrost, they are at least associated with periglacial processes. Despite the erosive warm, wet interglacial climate and dense vegetation that can obscure and erode past permafrost features of places such as the Mid-Atlantic Coastal Plain, periglacial features such as sand-wedge casts, solifluction, colluvium deposits, rock streams, block streams, talus, and rubble sheets are provided as evidence (French and Millar, 2014; Merritts and Rahnis, 2022), though these features are not strictly associated with permafrost and can form where there is deep seasonal frost (Ballantyne and Harris, 1994; Wolfe et al., 2018). These features, largely dating to the LGM, are found along the southern margins of the Laurentide Ice Sheet with a broader extent in eastern North America and slightly narrower extent in the Interior Great Plains (French and Millar, 2014).

Ice wedge pseudomorphs, and relict sand wedges of LGM age, are restricted to the area immediately south of the Laurentide margin, such as New Jersey, Pennsylvania, and in the northern midwest, as well as high-altitude locations of the Rocky Mountains in the American West. Traces of thermal contraction polygon networks have been found through aerial imagery in crop fields of southern New Jersey and the Delmarva Peninsula (Gao, 2014) and in the northern Valley and Ridge region of the Appalachian Mountains (Merritts and Rahnis, 2022). The presence of sand wedges in a gravel substrate in Delaware and Maryland suggests at least deep seasonal thawing (French et al., 2003) under arid conditions. Distinguishing between perennial and deep seasonal frost, however is problematic and permafrost, if present in the mid-Atlantic, would have been discontinuous or sporadic at best (French et al., 2009). Furthermore, features such as ice wedges and polygonal ground are largely restricted to the continuous permafrost zone (French and Millar, 2014) and therefore would not have been present in this region, regardless (French et al., 2009).
Ice wedge pseudomorphs younger than the LGM are recorded from within the southern limit of the Laurentide Ice sheet in the upper Midwest, southwestern New York, and southern New England, indicating their formation following initial ice sheet retreat, which can provide insights into paleoclimate and rates of retreat. In Canada, post-LGM ice wedge pseudomorphs are described from Alberta to the east of the Rockies, northern Saskatchewan, and Québec (French and Millar, 2014). In Alaska, LGM ice wedge pseudomorphs and/or syngenetic ice or sand wedges from unglaciated portions of Alaska are recorded as far south as the southern Bering Sea in former Beringia (French and Millar, 2014).

3.6. Qinghai-Tibet Plateau

On the Qinghai-Tibet Plateau, permafrost development can be assumed for two Middle Pleistocene periods (780-550 ka and 480-420 ka) in the vicinity of glaciers each followed by thawing in the subsequent interglacial periods (Chang et al., 2017). Direct evidence of past permafrost formation was found for the penultimate glacial period (150-130 ka), for the last glacial period (80-50 ka), and for the LGM (30-14 ka), each of which was followed by a thawing of the permafrost (Chang et al., 2017).
Traces of past permafrost of LGM age in China can be found particularly in the northeastern mountains and on the Qinghai-Tibet Plateau (Zhao et al., 2014; Lindgren et al., 2016; Vandenberghe et al., 2020). The main periglacial features are sand wedges, most of which have been dated by OSL between 23 and 17 ka. Since sand wedges can be up to 3 m deep, the authors consider that they were formed in association with permafrost in an arid context. Their distribution suggests that LGM permafrost extended as far as latitude 31°N on the Qinghai-Tibet plateau at an altitude above ca. 4000 m a.s.l. and 39°N in northeast China at an altitude above 2000 m a.s.l.

4. Summary and conclusions

Ancient and past permafrost sites are present in several regions of the Arctic and represent indicators of long-term permafrost and climate developments. These sites contain paleo-environmental archives with varying paleo-information recorded in sediments, ground ice, cave deposits, paleontological remains, isotopic and biogeochemical proxies, as well as in landforms. Such permafrost paleoenvironmental archives are valuable and can inform about the response of permafrost, e.g., formation, stability, and degradation, to past climate variations.
The discussed evidence clearly indicates that permafrost and its dynamics have been an important phenomenon of the high northern latitudes since the late Pliocene, particularly in

regions that were not glaciated during the Pleistocene. While initially several periods of major regional permafrost formation and thaw can be inferred for the late Pliocene and Early Pleistocene, before permafrost became more persistent and widely distributed across the Arctic during the Middle and Late Pleistocene. Even though new and further developed dating methods are increasingly improving the chronology of ancient and past permafrost for many deposits, the current chronological classification is still coarse and remains limited by sparse sites, regional gaps, and the age range and uncertainties of dating methods. Hence, to better place permafrost deposits and the inferred paleoenvironmental information in time, more and systematic dating of ancient and past permafrost in exposures and cores is crucial, preferentially using different independent methods that allow cross-validation. Ancient and past permafrost archives can be used to derive climatic thresholds for long-term, broad-scale permafrost dynamics, considering the (1) seasonality of temperature and precipitation, (2) continentality (distance to oceanic moisture and vast ice sheets), and (3) local soil, vegetation cover, fauna, geomorphology, hydrology, and disturbances. Therefore, studying ancient and past permafrost may provide suitable comparisons and analogues for current and future climate warming. In this context, it is worth noting that ancient permafrost – under certain local conditions – has survived interglacials that were warmer (MIS 5e) or longer (MIS 11) than the Holocene, which may provide insights into the future of permafrost under anthropogenic warming trajectories. In this context, the storage capacity of ancient permafrost for carbon and nitrogen, as well as ancient life, viruses, and DNA preserved in ancient permafrost, underlines the importance of better understanding past permafrost dynamics and its records in paleoenvironmental archives.

References

Abramov, A., Vishnivetskaya, T., Rivkina, E., 2021. Are permafrost microorganisms as old as permafrost? FEMS Microbiol. Ecol. 97, fiaa260, https://doi.org/10.1093/femsec/fiaa260.

Alempic, J.-M., Lartigue, A., Goncharov, A.E., Grosse, G., Strauss, J., Tikhonov, A.N., Fedorov, A.N., Poirot, O., Legendre, M., Santini, S., Abergel C., Claverie, J.-M. 2023. An Update on Eukaryotic Viruses Revived from Ancient Permafrost. Viruses 15, 564, https://doi.org/10.3390/v15020564.

Andrieux, E., Bateman, M., Bertran, P., 2018. The chronology of Late Pleistocene thermal contraction cracking derived from sand wedge dating in central and southern France. Glob. Planetary Change 162, 84-100, https://doi.org/10.1016/j.gloplacha.2018.01.012.

Andrieux, E., Bertran, P., Saito, K., 2016. Spatial analysis of the French Pleistocene permafrost by a GIS database. Permafr. Periglac. Process. 27, 17-30, https://doi.org/10.1002/ppp.1856.

Ashastina, K., Kuzmina, S., Rudaya, N., Troeva, E., Schoch, W.H., Römermann, C., Reinecke, J., Otte, V., Savvinov, G., Wesche, K., Kienast, F. 2018. Woodlands and steppes: Pleistocene vegetation in Yakutia's most continental part recorded in the Batagay permafrost sequence. Quat Sci Rev 196, 38-61, https://doi.org/10.1016/j.quascirev.2018.07.032.

Astakhov V. I., Kaplyanskaya F. A., Tarnogradsky V. D., 1996. Pleistocene Permafrost of West Siberia as a deformable glacier bed. Permafr. Periglac. Process. 7, 165–191, https://doi.org/10.1002/(SICI)1099-1530(199604)7:2<165::AID-PPP218>3.0.CO;2-S

Ballantyne, C.K., Harris, C., 1994. The Periglaciation of Great Britain. Cambridge University Press, Cambridge, https://doi.org/10.1002/jqs.3390100112.

Bartolomé M., Luetscher M., Spötl C., Cazenave G., Osácar M.C., Belmonte A., Cheng H., Edwards R.L., Sancho C., Moreno A., 2022. Coarse cryogenic cave carbonate formation over last 16,000 years in Devaux cave (Central Pyrenees). Climate Change: The Karst Record IX (KR9), July 17th-20th, 2022, University of Innsbruck, Austria. 90-91.

Batchelor, C.L., Margold, M., Krapp, M., Murton, D.K., Dalton, A.S., Gibbard, P.L., Stokes, C.R., Murton, J.B., Manica, A., 2019. The configuration of Northern Hemisphere ice sheets through the Quaternary. Nat Commun 10, 3713, https://doi.org/10.1038/s41467-019-11601-2

Bertran, P., 2022. Distribution and characteristics of Pleistocene ground thermal contraction polygons in Europe from satellite images. Permafr. Periglac. Process. 33, 99-113, https://doi.org/10.1002/ppp.2137.

Bertran, P., Stadelmaier, K.H., Ludwig, P., 2022. Last Glacial Maximum active layer thickness in Western Europe, and the issue of ‘tundra gleys’ in loess sequences. J Quat Sci 37, 1222-1228, https://doi.org/10.1111/bor.12049.

Biller-Celander, N., Shakun, J.D., McGee, D., Wong, C.I., Reyes, A.V., Hardt, B., Tal, I., Ford, D.C., Lauriol, B., 2021. Increasing Pleistocene permafrost persistence and carbon cycle conundrums inferred from Canadian speleothems. Sci. Adv. 7, eabe5799, https://doi.org/10.1126/sciadv.abe5799.

Blinov A., Alfimov, V., Beer, J., Gilichinsky, D., Schirrmeister, L., Kholodov, A., Nikolskiy, P., Opel, T., Tikhomirov, D., Wetterich, S., 2009. Ratio of 36Cl/Cl in ground ice of east Siberia and its application for chronometry. Geochemistry, Geophys. Geosystems 10, Q0AA03, https://doi.org/10.1029/2009GC002548.

Buylaert, J.P., Ghysels, G., Murray, A.S., Thomsen, K.J., Vandenberghe, D., De Corte, F., Heyse, I., Van den Haute, P., 2009. Optical dating of relict sand wedges and composite-

wedge pseudomorphs in Flanders, Belgium. Boreas 38, 160–175, https://doi.org/10.1111/j.1502-3885.2008.00037.x.

Cherbunina, M.Y., Karaevskaya, E.S., Vasil'chuk, Y.K., Tananaev, N.I., Shmelev, D.G., Budantseva, N.A., Merkel, A.Y., Rakitin, A.L., Mardanov, A.V., Brouchkov, A.V., Bulat, S.A., 2021. Microbial and Geochemical Evidence of Permafrost Formation at Mamontova Gora and Syrdakh, Central Yakutia. Front. Earth Sci. 9, 1020, https://doi.org/10.3389/feart.2021.739365.

Chang, X.L., Jin, H.J., He, R.X., Lü, L.Z., Harris, S.A., 2017. Evolution and changes of permafrost on the Qinghai-Tibet Plateau during the Late Quaternary. Sci. Cold Arid. Reg. 9, 1-19, https://doi.org/10.1007/s11430-018-9272-0.

Courtin, J., Perfumo, A., Andreev, A., Opel, T., Stoof-Leichsenring, K., Edwards, M., Murton, J.B., Herzschuh, U., 2022. Pleistocene glacial and interglacial ecosystems inferred from ancient DNA analyses of permafrost sediments from Batagay megaslump, East Siberia. Environ. DNA 4, 1265-1283, https://doi.org/10.1002/edn3.336.

Eissmann, L., 2002. Quaternary geology of eastern Germany (Saxony, Saxon–Anhalt, South Brandenburg, Thuringia), type area of the Elsterian and Saalian Stages in Europe, Quat Sci Rev 21, 1275–1346, https://doi.org/10.1016/S0277-3791(01)00075-0.

Elias, S.A. (Eds.), 2024. Encyclopedia of Quaternary Science, third ed. Elsevier Science.

Ewing, S.A., Paces, J.B., O'Donnell, J.A., Jorgenson, M.T., Kanevskiy, M.Z., Aiken, G.R., Shur, Y., Harden, J.W., Striegl, R., 2015. Uranium isotopes and dissolved organic carbon in loess permafrost: Modeling the age of ancient ice. Geochim. Cosmochim. Acta 152, 143-165, https://doi.org/10.1016/j.gca.2014.11.008.

Farkas, B., Sipos, G., Bartyik, T., Józsa, E., Czigány, S., Balogh, R., Varga, G., Kovács, J., Fábián, S.A., 2023. Characterization and mapping of MIS-2 thermal contraction crack polygons in Western Transdanubia, Hungary. Permafr. Periglac. Process. 34, 417–427, https://doi.org/10.1002/ppp.2190.

French, H.M., Millar, S.W.S., 2014. Permafrost at the time of the Last Glacial Maximum (LGM) in North America. Boreas 43, 667-677, https://doi.org/10.1111/bor.12036.

French, H., Shur, Y., 2014. The principles of cryostratigraphy. Earth Sci Rev 101, 190-206, https://doi.org/10.1016/j.earscirev.2010.04.002.

Froese, D.G., Westgate, J.A., Reyes, A.V., Enkin, R.J., Preece, S.J., 2008. Ancient permafrost and a future, warmer arctic. Science 321, 1648-1648, https://doi.org/10.1126/science.1157525.

Gao, C., 2014. Relict thermal- contraction- crack polygons and past permafrost south of the Late Wisconsinan glacial limit in the mid- Atlantic Coastal Plain, USA. Permafr. Periglac. Process. 25, 144-149, https://doi.org/10.1002/ppp.1803

Germonpré, M., Fedorov, S., Danilov, P., Galeta, P., Jimenez, E. L., Sablin, M., Losey, R.J., 2017. Palaeolithic and prehistoric dogs and Pleistocene wolves from Yakutia: Identification of isolated skulls. J. Archaeol. Sci. 78, 1-19, https://doi.org/10.1016/j.jas.2016.11.008.

Gilichinsky, D.A., 2002. Permafrost Model of Extraterrestrial Habitat, in: n: Horneck, G., Baumstark-Khan, C. (eds) Astrobiology. Springer, Berlin, Heidelberg, pp. 125-142, https://doi.org/10.1007/978-3-642-59381-9_9

Giterman, R. E., Sher, A. V., Matthews, J. V., 1982. Comparison of the Development of Tundra-Steppe Environments in West and East Beringia: Pollen and Macrofossil Evidence from Key Sections, in: Hopkins, D.M., Matthews, J.V., Schweger, C.E., Young, S.B. (Eds.),

Paleoecology of Beringia. Academic Press, New York, pp. 43–73, https://doi.org/10.1016/b978-0-12-355860-2.50011-9

Guo, D., Wang, H., Romanovsky, V.E., Haywood, A.M., Pepin, N., Salzmann, U., Sun, J., Yan, Q., Zhang, Z., Li, X., Otto-Bliesner, B.L., Feng, R., Lohmann, G., Stepanek, C., Abe-Ouchi, A., Chan, W.-L., Peltier, W.R., Chandan, D., von der Heydt, A.S., Contoux, C., Chandler, M.A., Tan, N, Zhang, Q., Hunter, S.J., Kamae, Y., 2023. Highly restricted near-surface permafrost extent during the mid-Pliocene warm period. Proc. Natl. Acad. Sci. U.S.A. 120, e2301954120, https://doi.org/10.1073/pnas.2301954120.

Gusev, E.A., Kostin, D.A., Rekant, P.V., Sharin, V.V., Dorechkina D.E., Zarkhidze, D.V., 2012a. Problems of the mapping and genetic interpretation of the Russian Arctic shelf Quaternary deposits. Regional geology and metallogeny 50, 5-14 (in Russian).

Gusev, E. A., Krylov, A. V., Voronkov, A. Yu. & Nikitin, M. Y., 2012b. Pleistocene-Holocene molluscs of the Yenisseian North. in Avetisov, G. P. (Ed.), Geological and Geophysical Features of Lithosphere of Arctic Region/Transactions of VNIIOkeangeologia 223, 75–85 (in Russian with English summary).

Isarin, R., Huijzer, B., van Huissteden, K., 1998. Time-slice oriented multiproxy database (MPDB) for palaeoclimatie reconstruction. National Snow and Ice Data Center, University of Boulder, Colorado. http://nsidc. org/data/ggd248.html.

Jensen, B.J.L., Reyes, A.V., Froese, D.G., Stone, D.B., 2013. The Palisades is a key reference site for the middle Pleistocene of eastern Beringia: new evidence from paleomagnetics and regional tephrostratigraphy. Quat Sci Rev 63, 91-108, https://doi.org/10.1016/j.quascirev.2012.11.035.

Jones, M.C., Grosse, G., Treat, C., Turetsky, M., Anthony, K.W., Brosius, L., 2023. Past permafrost dynamics can inform future permafrost carbon-climate feedbacks. Commun. Earth Environ. 4, 272, https://doi.org/10.1038/s43247-023-00886-3.

Kanevskiy, M., Shur, Y., Bigelow, N.H., Bjella, K.L., Douglas, T.A., Fortier, D., Jones, B.M. and Jorgenson, M.T., 2022. Yedoma cryostratigraphy of recently excavated sections of the CRREL permafrost tunnel near Fairbanks, Alaska. Front. Earth Sci. 9, https://doi.org/10.3389/feart.2021.758800.

Kanevskiy, M., Shur, Y., Fortier, D., Jorgenson, M.T. and Stephani, E., 2011. Cryostratigraphy of late Pleistocene syngenetic permafrost (yedoma) in northern Alaska, Itkillik River exposure. Quat Res *75*, 584-596. https://doi.org/10.1016/j.yqres.2010.12.003

Kienast, F., Wetterich, S., Kuzmina, S., Schirrmeister, L., Andreev, A.A., Tarasov, P., Nazarova, L., Kossler, A., Frolova, L., Kunitsky, V.V., 2011. Paleontological records indicate the occurrence of open woodlands in a dry inland climate at the present-day Arctic coast in western Beringia during the Last Interglacial. Quat Sci Rev 30, 2134-2159, https://doi.org/10.1016/j.quascirev.2010.11.024.

Kokelj, S., Lantz, T.,Wolfe, S.A., Kanigan, J., Morse, P., Coutts, R., Molina-Giraldo, N., Burn, C.R., 2014. Distribution and activity of ice wedges across the forest-tundra transition, western Arctic Canada, J. Geophys. Res. Earth 119, 2032–2047, https://doi.org/10.1002/2014JF003085.

Kokelj, S.V., Pisaric, M.F.J., Burn, C.R., 2007. Cessation of ice-wedge development during the 20th century in spruce forests of eastern Mackenzie Delta, Northwest Territories, Canada. Can J Earth Sci 44, 1503–1515, https://doi.org/10.1139/e07-035.

Lindgren, A., Hugelius, G., Kurhy, P., Christensen, T.R., Vandenberghe, J., 2016. GIS-based Maps and Area Estimates of Northern Hemisphere Permafrost Extent during the Last Glacial Maximum. Permafr. Periglac. Process. 27, 1-16, https://doi.org/10.1002/ppp.1851.

Łozi´nski W., 1912. Die periglaciale Fazies der mechanischen Verwitterung, in: Comptes Rendus XII Int Geol Congr, Stockholm, pp. 1039–1053.

Ludwig, P., Gómez-Navarro, J.J., Pinto, J.G., Raible, C.C., Wagner, S., Zorita, E., 2019. Perspectives of regional paleoclimate modeling. Ann. N. Y. Acad. Sci. 1436, 54-69, https://doi.org/10.1111/nyas.13865.

Matheus, P., Begét, J., Mason, O. and Gelvin-Reymiller, C., 2003. Late Pliocene to late Pleistocene environments preserved at the Palisades site, central Yukon River, Alaska. Quat Res 60, 33-43, https://doi.org/10.1016/S0033-5894(03)00091-7

Matsuoka, N., Christiansen, H.H., Watanabe, T., 2018. Ice- wedge polygon dynamics in Svalbard: Lessons from a decade of automated multi- sensor monitoring. Permafr. Periglac. Process. 29, 210-227, https://doi.org/10.1002/ppp.1985.

Meijs, E.P.M., 2011. The Veldwezelt site (province of Limburg, Belgium): environmental and stratigraphical interpretations. NETH J GEOSCI 90.2-3, 73-94, https://doi.org/10.1017/S0016774600001037.

Merritts, D.J. and Rahnis, M.A., 2022. Pleistocene Periglacial Processes and Landforms, Mid-Atlantic Region, Eastern United States. Annu. Rev. Earth Planet. 50, 541-592, https://doi.org/10.1146/annurev-earth-032320-102849

Miner, K.R., Hollis, J.R., Miller, C.E., Uckert, K., Douglas, T.A., Cardarelli, E., Mackelprang, R., 2023. Earth to Mars: A Protocol for Characterizing Permafrost in the Context of Climate Change as an Analog for Extraplanetary Exploration. Astrobiology 23, 1006-1018, https://doi.org/10.1089/ast.2022.0155.

Miner, K.R., D'Andrilli, J., Mackelprang, R., Edwards, A., Malaska, M.J., Waldrop, M.P. and Miller, C.E., 2021. Emergent biogeochemical risks from Arctic permafrost degradation. Nat. Clim. Change 11, 809-819, https://doi.org/10.1038/s41558-021-01162-y.

Moseley, G.E., Edwards, R.L., Lord, N.S., Spötl, C., Cheng, H., 2021. Speleothem record of mild and wet mid-Pleistocene climate in northeast Greenland. Sci. Adv. 7, eabe1260, https://doi.org/10.1126/sciadv.abe1260.

Murton, J.B., Opel, T., Toms, P., Blinov, A., Fuchs, M., Wood, J., Gärtner, A., Merchel, S., Rugel, G., Savvinov, G., Wetterich S., 2022. A multimethod dating study of ancient permafrost, Batagay megaslump, east Siberia. Quat Res 105, 1-22, https://doi.org/10.1017/qua.2021.27.

Murton, J.B., 2021. What and where are periglacial landscapes? Permafr. Periglac. Process. 32, 186-212, https://doi.org/10.1002/ppp.2102.

Nazarov, D.V., Nikolskaia, O.A., Gladysheva, A.S., Zhigmanovskiy, I.V., Ruchkin, M.V., Merkuljev, A.V. and Thomsen, K.J., 2022. Evidence for the intrusion of marine Atlantic waters into the West Siberian Arctic during the Middle Pleistocene. Boreas 51, 402-425, https://doi.org/10.1111/bor.12558.

Nelson, F.E., Outcalt, S.I., 1987. A Computational Method for Prediction and Regionalization of Permafrost. Arct. Alp. Res. 19, 279-288, https://doi.org/10.1080/00040851.1987.12002602.

Obu, J., Westermann, S., Barboux, C., Bartsch, A., Delaloye, R., Grosse, G., Heim, B., Hugelius, G., Irrgang, A., Kääb, A.M., Kroisleitner, C., Matthes, H., Nitze, I., Pellet, C., Seifert, F.M., Strozzi, T., Wegmüller, U., Wieczorek, M., Wiesmann, A., 2024. ESA Permafrost Climate Change Initiative (Permafrost_cci): Permafrost version 3 data products. Centre for Environmental Data Analysis, 29.02.2024. http://catalogue.ceda.ac.uk/uuid/8239d5f6263f4551bf2bd100d3ecbead

Okkonen, J., Neupauer, R., Kozlovskaya, E., Afonin, N., Moisio, K., Taewoo, K., Muurinen, E., 2020. Frost Quakes: Crack Formation by Thermal Stress, J. Geophys. Res. Earth 125, e2020JF005616, https://doi.org/10.1029/2020JF005616.

Oliva, M., Fernández-Fernández, J.M., Nývlt, D. (Eds.), 2022. Periglacial Landscapes of Europe. Springer International Publishing: Cham, Switzerland, https://doi.org/10.1007/978-3-031-14895-8.

Opel, T., Wetterich, S., Meyer, H., Dereviagin, A.Y., Fuchs, M.C., Schirrmeister, L., 2017. Ground-ice stable isotopes and cryostratigraphy reflect late Quaternary palaeoclimate in the Northeast Siberian Arctic (Oyogos Yar coast, Dmitry Laptev Strait). Clim. Past 13, 587-611, https://doi.org/10.5194/cp-13-587-2017.

Pavlidis, Yu.A., Dunaev, N.N., Shcherbakov, F.A., 1997. The late pleistocene palaeogeography of Arctic Eurasian shelves. Quat. Int. 41-42, 3-9, https://doi.org/10.1016/S1040-6182(96)00030-4.

Péwé, T.L., Westgate, J.A., Preece, S.J., Brown, P.M., Leavitt, S.W., 2009. Late Pliocene Dawson Cut Forest Bed and new tephrochronological findings in the Gold Hill Loess, east-central Alaska. Geol Soc Am Bull 121, 294-320, https://doi.org/10.1130/B26323.1.

Repenning, C.A., 1992. Allophaiomys and the age of the Olyor Suite, Krestovka Sections, Yakutia. US Geological Survey Bulletin 2037, 1-98.

Repenning, C.A., Brouwers, E.M., 1992. Late Pliocene-early Pleistocene ecologic changes in the Arctic Ocean Borderland. US Geological Survey Bulletin 2063, 1-37.

Reyes, A.V., Froese, D.G., Jensen, B.J.L., 2010. Permafrost response to last interglacial warming field evidence from non-glaciated Yukon and Alaska. Quat Sci Rev 29, 3256-3274, https://doi.org/10.1016/j.quascirev.2010.07.013.

Saito, K., Sueyoshi, T., Marchenko, S., Romanovsky, V., Otto-Bliesner, B., Walsh, J., Bigelow, N., Hendricks, A., Yoshikawa, K., 2013. LGM permafrost distribution: how well can the latest PMIP multi-model ensemble perform reconstruction? Clim. Past 9, 1697-1714, https://doi.org/10.5194/cp-9-1697-2013.

Schirrmeister, L., Froese, D., Wetterich, S., Straus, J., Veremeeva, A., Grosse, G. (this volume). Yedoma: Late Pleistocene ice-rich syngenetic permafrost of Beringia.

Schirrmeister, L., Meyer, H., Andreev, A., Wetterich, S., Kienast, F., Bobrov, A., Fuchs, M., Sierralta, M., & Herzschuh, U., 2016. Late Quaternary paleoenvironmental records from the Chatanika River valley near Fairbanks (Alaska). Quat Sci Rev 147, 259-278. https://doi.org/10.1016/j.quascirev.2016.02.009

Schirrmeister, L., Oezen, D., Geyh, M.A., 2002. 230 Th/U Dating of Frozen Peat, Bol'shoy Lyakhovsky Island (Northern Siberia). Quat Res 57, 253-258. https://doi.org/10.1006/qres.2001.2306

Seltzer, A.M., Ng, J., Aeschbach, W., Kipfer, R., Kulongoski, J.T., Severinghaus, J.P., Stute, M., 2021. Widespread six degrees Celsius cooling on land during the Last Glacial Maximum. Nature 593, 228-232, https://doi.org/10.1038/s41586-021-03467-6.

Sher, A.V., 1997. A brief overview of the Late-Cenozoic History of the Western Beringian Lowlands, in: Edwards, M.E., Sher, A.V., Guthrie, R.D. (ds.), Terrestrial Paleoenvironmental Studies in Beringia. Alaska Quaternary Center, University of Alaska Fairbanks, pp. 3-6.

Sher, A.V., Kaplina, T.N., Giterman, R.E., Lozhkin, A.V., Arkhangelow, A.A., Kiselyov, S.V., Kouznetsov, Yu.V., Virina, E.I., Zazhigin, V.S., 1979. Scientific Excursion on Problem “Late Cenozoic of the Kolyma Lowland”. Excursion Tour XI Guide-Book. Academy of Sciences, USSR XIV Pacific Science Congress, Moscow.

Sher, A.V., 1974. Pleistocene Mammals and Stratigraphy of the Far Northeast USSR and North America. International Geological Review 16.

Shmelev, D., Veremeeva, A., Kraev, G., Kholodov, A., Spencer, R.G.M., Walker, W.S., Rivkina, E., 2017. Estimation and Sensitivity of Carbon Storage in Permafrost of North-Eastern Yakutia. Permafr. Periglac. Process. 28, 379–390, https://doi.org/10.1002/ppp.1933.

Shpolyanskaya, N.A., 2015. Pleistocene-Holocene history of the development of the Russian Arctic permafrost zone in terms of ground ice. MSU, Moscow-Izhevsk (in Russian).

Slater, A.G., Lawrence, D.M., 2013. Diagnosing Present and Future Permafrost from Climate Models. J. Clim. 26, 5608-5623, https://doi.org/10.1175/JCLI-D-12-00341.1.

Stadelmaier, K.H., Ludwig, P., Bertran, P., Antoine, P., Shi, X., Lohmann, G., Pinto, J.G., 2021. A new perspective on permafrost boundaries in France during the Last Glacial Maximum. Clim. Past 17, 2559-2576, https://doi.org/10.5194/cp-17-2559-2021.

Steffen, W., Richardson, K., Rockström, J., Schellnhuber, H.J., Dube, O.P., Dutreuil, S., Lenton, T.M., Lubchenco, J., 2020. The emergence and evolution of Earth System Science. Nat. Rev. Earth Environ. 1, 54-63, https://doi.org/10.1038/s43017-019-0005-6.

Strauss, J., Fuchs, M., Hugelius, G., Miesner, F., Nitze, I., Opfergelt, S., Schuur, E.., Treat, C., Turetsky, M., Yang, Y., Grosse, G. (this volume). Organic matter storage and vulnerability in the permafrost domain.

Streletskaya, I.D., Pismeniuk, A.A., Vasiliev, A.A., Gusev, E.A., Oblogov, G.E., Zadorozhnaya, N.A., 2021 The Ice-Rich Permafrost Sequences as a Paleoenvironmental Archive for the Kara Sea Region (Western Arctic). Front. Earth Sci. 9, 723382. https://doi.org/10.3389/feart.2021.723382.

Svendsen, J. I., Alexanderson, H., Astakhov, V. I., Demidov, I., Dowdeswell, J. A., Funder, S., Gataullin, V., Henriksen, M., Hjort, C., Houmark-Nielsen, M., Hubberten, H. W., Ingólfsson, Ó., Jakobsson, M., Kjær, K. H., Larsen, E., Lokrantz, H., Lunkka, J. P., Lysså, A., Mangerud, J., Matiouchkov, A., Murray, A., Möller, P., Niessen, F., Nikolskaya, O., Polyak, L., Saarnisto, M., Siegert, C., Siegert, M. J., Spielhagen, R. F., Stein, R., 2004. Late Quaternary ice sheet history of northern Eurasia, Quat Sci Rev 23, 1229-1271, https://doi.org/10.1016/j.quascirev.2003.12.008, 2004.

Treat, C.C. and Jones, M.C., 2018. Near-surface permafrost aggradation in Northern Hemisphere peatlands shows regional and global trends during the past 6000 years. Holocene 28, 998-1010, https://doi.org/10.1177/0959683617752858

Vaks, A., Mason, A.J., Breitenbach, S.F.M., Kononov, A.M., Osinzev, A.V., Rosensaft, M., Borshevsky, A., Gutareva, O.S., Henderson, G.M., 2020. Palaeoclimate evidence of vulnerable permafrost during times of low sea ice. Nature 577, 221-225, https://doi.org/10.1038/s41586-019-1880-1.

Vaks, A., Gutareva, O.S., Breitenbach, S.F.M., Avirmed, E., Mason, A.J., Thomas, A.L., Osinzev, A.V., Kononov, A.N., Henderson, G.M., 2013. Speleothems Reveal 500,000-Year History of Siberian Permafrost. Science 340, 183-186, https://doi.org/10.1126/science.1228729.

Vandenberghe, J., French, H., Jin, H., Wang, X., Yi, S., He, R., 2020. The impact of latitude and altitude on the extent of permafrost during the Last Permafrost Maximum (LPM) in North China. Geomorphology 350, 106909, https://doi.org/10.1016/j.geomorph.2019.106909.

Vandenberghe, J., French, H.M., Gorbunov, A., Marchenko, S., Velichko, A.A., Jin, H., Cui, H., Zhang, T., Wan, X., 2014. The Last Permafrost Maximum (LPM) map of the Northern

Hemisphere: permafrost extent and mean annual air temperatures, 25-17 ka BP. Boreas 43, 652-666, https://doi.org/10.1111/bor.12070.

Vandenberghe, J., Rennssen, H., Roche, D.M., Goosse, H., Velichko, A.A., Gorbunov, A., Levavasseur, G., 2012. Eurasian permafrost instability constrained by reduced sea-ice cover. Quat Sci Rev 34, 16-23, https://doi.org/10.1016/j.quascirev.2011.12.001.

van der Valk, T., Pečnerová, P., Díez-del-Molino, D., Bergström, A., Oppenheimer, J., Hartmann, S., Xenikoudakis, G., Thomas, J.A., Dehasque, M., Sağlıcan, E., Fidan, F.R., Barnes, I., Liu, S., Somel, M., Heinthman, P.D., Nikolskiy, P., Shapiro, B., Skoglund, P., Hofreiter, M., Lister, A.M., Götherström, A., Dalén, L., 2021. Million-year-old DNA sheds light on the genomic history of mammoths. Nature 591, 265–269, https://doi.org/10.1038/s41586-021-03224-9.

Verret. M., Dickinson, W., Lacelle, D., Fisher, D., Norton, K., Chorley, H., Levy, R., Naish, T., 2021. Cryostratigraphy of mid-Miocene permafrost at Friis Hills, McMurdo Dry Valleys of Antarctica. Antarctic Science 33, 174-188. https://doi.org/10.1017/S0954102020000619

Wennrich, V., Andreev, A.A., Tarasov, P.E., Fedorov, G., Zhao, W., Gebhardt, C.A., Meyer-Jacob, C., Snyder, J.A., Nowaczyk, N.R., Schwamborn, G., Chapligin, B., Anderson, P.M., Lozhkin, A.V., Minyuk, P.S., Koeberl, C., Melles, M., 2016. Impact processes, permafrost dynamics, and climate and environmental variability in the terrestrial Arctic as inferred from the unique 3.6 Myr record of Lake El'gygytgyn, Far East Russia – A review. Quat Sci Rev 147, 221-244, https://doi.org/10.1016/j.quascirev.2016.03.019.

Westgate, J., Froese, D.G., 2001. Stop 15: Quartz Creek: Pliocene ice wedges/Quartz Creek tephra (63 46’ N, 139 03’ W). In: Froese, D.G., Duk-Rodkin, A., Bond, J.D. (Eds.), Fieldguide to Quaternary Research in central and western Yukon Territory. Yukon Heritage Branch Occasional Papers in Earth Science 2, 69-71.

Wetterich, S., Rudaya, N., Kuznetsov, V., Maksimov, F., Opel, T., Meyer, H., Günther, F., Bobrov, A., Raschke, E., Zimmermann, H.H., Strauss, J., Starikova, A., Fuchs, M., Schirrmeister, L., 2019. Ice Complex formation on Bol'shoy Lyakhovsky Island (New Siberian Archipelago, East Siberian Arctic) since about 200 ka. Quat Res 92, 530-548, https://doi.org/10.1017/qua.2019.6.

Wetterich, S., Tumskoy, V., Rudaya, N., Kuznetsov, V., Maksimov, F., Opel, T., Meyer, H., Andreev, A.A., Schirrmeister, L., 2016. Ice Complex permafrost of MIS5 age in the Dmitry Laptev Strait coastal region (East Siberian Arctic). Quat Sci Rev 147, 298-311, https://doi.org/10.1016/j.quascirev.2015.11.016.

Willerslev, E., Davison, J., Moora, M., Zobel, M., Coissac, E., Edwards, M. E., Lorenzen, E. D., Vestergård, M., Gussarova, G., Haile, J., Craine, J., Gielly, L., Boessenkool, S., Epp, L. S., Pearman, P. B., Cheddadi, R., Murray, D., Bråthen, K. A., Yoccoz, N., Binney, H., Cruaud, C., Wincker, P., Goslar, T., Alsos, I. G., Bellemain, E., Brysting, A. K., Elven, R., Sønstebø, J. H., Murton, J., Sher, A., Rasmussen, M., Rønn, R., Mourier, T., Cooper, A., Austin, J., Möller, P., Froese, D., Zazula, G., Pompanon, F., Rioux, D., Niderkorn, V., Tikhonov, A., Savvinov, G., Roberts, R. G., MacPhee, R. D. E., Gilbert, M. T. P., Kjær, K. H., Orlando, L., Brochmann, C., Taberlet, P., 2014. Fifty thousand years of Arctic vegetation and megafaunal diet. Nature 506, 47-51. https://doi.org/10.1038/nature12921.

Wolfe, S.A., Morse, P.D., Neudorf, C.M., Kokelj, S.V., Lian, O.B., O'Neill, H.B., 2018. Contemporary sand wedge development in seasonally frozen ground and paleoenvironmental implications. Geomorphology 308, 215-229, https://doi.org/10.1016/j.geomorph.2018.02.015.

Žák, K., Richter, D.K., Filippi, M., Živor, R., Deininger, M., Mangini, A., Scholz, D., 2012. Coarsely crystalline cryogenic cave carbonate – a new archive to estimate the Last Glacial minimum permafrost depth in Central Europe. Clim Past 8, 1821-1837, https://doi.org/10.5194/cp-8-1821-2012.

Zech, M., Tuthorn, M., Detsch, F., Rozanski, K., Zech, R., Zöller, L., Zech, W., Glaser, B., 2013. A 220ka terrestrial $\delta^{18}O$ and deuterium excess biomarker record from an eolian permafrost paleosol sequence, NE-Siberia. Chem. Geol. 360-361, 220-230, https://doi.org/10.1016/j.chemgeo.2013.10.023.

Zemtsov, A.A., Shamakhov, A.F., 1993. Characteristics of relict permafrost on the West Siberian Plain, Polar Geography and Geology 17, 245-250, https://doi.org/10.1080/10889379309377522.

Zhao, L., Jin, H., Li, C., Cui, Z., Chang, X., Marchenko, S.S., Vandenberghe, J., Zhang, T., Luo, D., Guo, D., Liu, G., Yi, C., 2014. The extent of permafrost in China during the local Last Glacial Maximum (LLGM). Boreas 43, 688–698, https://doi.org/10.1111/bor.12049.